TOWARDS A UV DETECTOR FOR MICROFLUIDIC DEVICES

by

AMITA SHARMA

M.S., Tribhuvan University, Kathmandu, Nepal, 2010
B.S., Tri-Chandra Campus, Kathmandu, Nepal, 2006

A THESIS

Submitted in partial fulfillment of the requirements for the degree

MASTER OF SCIENCE

Department of Chemistry
College of Arts and Sciences

KANSAS STATE UNIVERSITY
Manhattan, Kansas

2013

Approved by:

Major Professor
Christopher T. Culbertson

Copyright

Abstract

Chemists have been trying to relate the structure and composition of different cereal proteins to their physical properties to better inform their product use for more than 250 years now[1]. Among these cereals, wheat is considered the most important due to its unique ability to form viscoelastic dough and retain gas during fermentation, the latter being important for bread making. This property is due to the endosperm part of wheat that contains proteins mostly gliadins and glutens. It is known that the composition and relative ratio of these proteins is determined by both the growing environment and genetics. Manipulation of the genetics allows one for control of only about 50% of the end use quality of the wheat and the rest is controlled by environment. Currently, the bread making quality of wheat is determined by baking test loaves of bread. This process is time consuming and wasteful. The main goal of this project was to create fingerprints of gliadin proteins for different wheat cultivars as a function of environmental conditions. This would then allow wheat kernels to be analyzed and assessed right after harvest to determine their appropriateness for making the various wheat products.

Researchers have tried to create a catalogue of information for individual wheat cultivars by 'fingerprinting' the gliadins proteins in wheat[2] using various analytical techniques including capillary electrophoresis (CE). CE offers advantages like high separation efficiency, and faster analysis. Further miniaturization of CE on microfluidic devices has enhanced the speed and efficiency of separation. Furthermore, it is possible to integrate multiple chemical analysis processes like sample preparation, separation and detection in a single microfluidics device[3]. Microfluidic uses micron sized separation channels defined in a glass, quartz or polymer. This dissertation is focused on fabricating multilayer microfluidic devices from Poly(dimethylsiloxane) (PDMS) and using these devices to electrophoretically separate wheat

gliadin proteins followed by detection using UV absorption in less than 5 min. PDMS is cheap, easy to fabricate and is optically transparent above ~230nm. Initial results of the UV absorbance detector developed for this device are presented.

Table of Contents

List of Figures

List of Tables

Acknowledgements

I would like to take this opportunity to thank everyone who helped me during my completion of graduate study. First of all I would like to thank Dr. Culbertson for his help and support and for taking time to discuss about work.

The Culbertsons Group, I really enjoyed working with all of you. Thanks for making all my time here enjoyable and homely.

My friends Eve, Amos, Mukund, Damith…I appreciate all the good times spent with you talking about nothing. Special thanks to my friend Eve, who was always there for me to help me in any problems.

I would like to thank my committee members Dr. Daniel Higgins and Dr. Jun Li.

I would also like to thank Earline Dikeman, Mary Dooley, and Kim Ross for their help.

To the faculty and staff of the chemistry department, thank for providing an environment friendly enough to complete my study. I would also like to thank chemistry department staffs Ron Jackson, Tobbe Eggers, Jim Hodgson.

At last, a big thanks to my husband Bhanu Neupane for supporting me emotionally and to my dear son Aryav Neupane for being a quiet, lovely boy.

Dedication

I would like to dedicate this thesis to my parents – my dad Yadunath Lamsal and my mom Chandrawati Sharma (Lamsal).

1 Introduction to Capillary Electrophoresis

1.1.Background on Electrophoresis

Electrophoresis is defined as the differential migration of charged species under a constant applied electric field. Electrophoresis was first coined by Michaelis in 1909 when he demonstrated the first separation of proteins based on their iso-electric points[4]. But the pioneering experiment demonstrating the separation of a mixture of proteins based upon their charge/mass ratios using was demonstrated by Tiselius in 1937[5]. This experiment was performed in a tube filled with buffer solutions. The mixture of proteins was placed at one end of tube and voltage applied across the two tube ends. Since his experiments were limited by thermal diffusion and convection, anti-convective media such as polyacrylamide gels were developed. Gels in a slab format have since emerged as the most efficient way of performing electrophoretic protein separations. But this technique also suffered from difficulties in detection, longer analysis time, and tedious sample preparation steps. More recently, electrophoresis in narrow tubes or capillaries has been developed as an alternative to slab gels. In the early 1970s, 2D electrophoresis was described by Dale and Latner[6] and Macko and Stegmann[7]. They performed iso-electric focusing (IEF) separation followed by PAGE (Polyacrylamide Gel Electrophoresis), where polyacrylamide gels were used for the separation and determination of proteins. Meanwhile in the pharmaceutical field, chemists were developing HPLC (High Performance Liquid Chromatography) which proved to be ideal for analysis of small molecules with speed and high resolution. Both HPLC and Electrophoresis failed to meet the demands of biotechnological research concerning gene cloning, protein expression due to poor resolution and the inability to separate molecules of larger size. Different chromatographic techniques were

developed but none of them were viable for commercial development due to high operating costs, high pressure handling problems and tedious sample preparation steps[8,9]. To overcome these problems, Hjerten used CE for the analysis of different analytes ranging from micro to macromolecular structures. He conducted CE in a 3 mm inner diameter tube[10]. Then, in the late 1970s/early 1980s Mikker et al.[11] and Jorgenson and Lukacs[12] reported CE as a viable analytical technique by demonstrating high efficiency separations in 75-um id fused silica capillaries using only nanoliter sample volumes. After this, CE was used in the analysis, separation and detection of polymers as well as small molecules providing high resolution with minimum sample/reagent use.

1.2. Capillary Electrophoresis: Theory, Principles and Applications

Separation is one of the main goals of most sample analysis problems conducted in the fields of chemistry, biology and other sciences. There are a number of different separation techniques, among which electrophoresis has emerged as a powerful tool. Traditional gel electrophoresis uses some kind of solid supports such as polyacrylamide or agarose gels as a convective media to improve separations. However, traditional forms of electrophoresis have many disadvantages including longer separation time, poor heat dissipation, and low separation efficiency. To overcome these problems, capillary electrophoresis was introduced. Capillary Electrophoresis (CE), also known as Capillary Zone Electrophoresis (CZE) or High Performance Capillary Electrophoresis (HPCE) offers many advantages including high separation efficiency, short analysis time, simple setup, and small sample consumption. Another advantage of CE is the high surface to volume ratio of capillaries. This allows for efficient heat dissipation which facilitates for the application of high electric fields. The use of different buffers increases the selectivity of

CE.[13] CE can be coupled to many detection systems such as Laser Induced Fluorescence (LIF), Mass Spectrometers (MS), UV-Visible Absorption, Conductivity and Refractive Index.

A proper definition of CE would be: "A separation method based on the differential migration of different ions under a constant applied electric field carried out in a narrow diameter capillary filled with buffer[14,15]". Differences in solute velocities due to the differences in their charge upon the application of electric field are the basis of separation in CE.

When an electric field is applied along the capillary, ions migrate at a velocity proportional to the field strength. This electrostatic force can be given as:

(1.1) $$F_e = qE$$

where, q is the charge of an analyte /ion and E is the electric field strength. The electric field is a function of the applied voltage (V) in volts to the capillary length (L) in centimeters. i.e.:

(1.2) $$E = \frac{V}{L}$$

This electric force is countered by the viscous forces that are inherent in the electrolyte solution. According to Stoke's law, the viscous force experienced by a spherical particle is given as:

(1.3) $$F_f = -6\pi\eta r\nu$$

Where, η is the solution viscosity, r is the ion radius, and ν is the electrophoretic velocity of the particle. These two forces reach a steady state as soon as voltage is applied where both are equal and opposite. i.e.:

$$F_f = F_e$$

Or, $qE = 6\pi\eta r\nu$

(1.4) $$\nu = \frac{qE}{6\pi\eta r}$$

An electrophoretic mobility (μ_e) is defined as:

(1.5) $$\mu_e = \frac{\nu}{E} = \frac{q}{6\pi\eta r}$$

It can be seen from this equation that size and charge of an analyte are major factors in determining mobility. Thus, analytes are separated by their effective charge to size ratio. Cations with larger charge to mass ratios will travel faster towards the cathode than cations with smaller charge to mass ratios. The same holds true for anions moving towards the anode[16].

1.2.1. Electroosmotic Flow

The force is experienced by analytes from the flow of bulk liquid, called electro-osmotic flow (EOF). This is the main force responsible for the whole electrophoresis process. Neutral analytes migrate with the speed of EOF which is one of the fundamental mechanisms present in the electrokinetic systems. In CE, it arises as the bulk fluid flow that is generated upon the application of electric field in a capillary that is filled with electrolyte. Capillaries used in CE are made of fused silica that posses negative charge when in contact with an aqueous buffer. These negatively charged silanol groups along the capillary inner wall attract cationic species from the buffer. Now a layer of positively charged species forms on the wall where charge density decreases exponentially as the perpendicular distance from the capillary wall increases. This double layer formed closest to the silica surface is static and called Inner Helmholtz plane (IHP) or Stern layer. A second layer forms near this Stern layer which is mobile and is called Outer

Helmholtz plane (OHP) or diffuse layer. This process was first observed and studied by Helmholtz in the 1800s when he was doing an experiment on a glass tube filled with an aqueous salt solution[17].

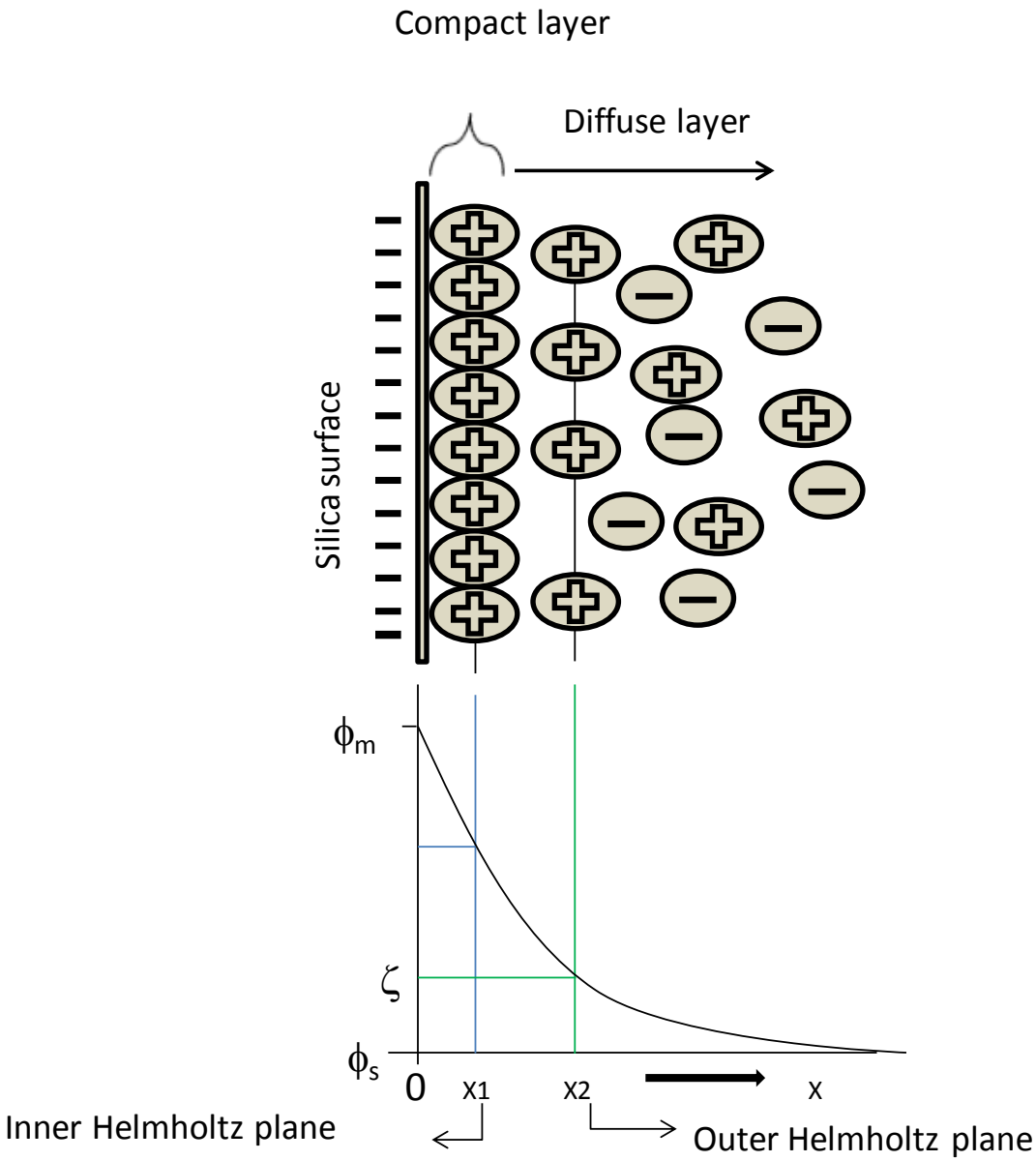

Figure 1-1: Electric double layer where "ϕ" is the electric potential due to the surface charge density. 'ζ' is the Zeta potential.

There is a potential difference established between the channel wall and bulk solution due to this electric double layer. This potential decreases as the distance from wall increases and is known as zeta potential[18]. When electric field is applied, hydrated cations in the solution move towards the cathode carrying the bulk of the buffer. The water molecules of the bulk solution also move due to the cohesive nature of water of hydration to this bulk water. This results in the entire bulk fluid flowing toward the cathode. This flow is called electro-osmotic flow. It acts as a pump propelling all molecules toward the detector depending on their respective electrophoretic mobility. EOF is for the most part beneficial but sometimes needs to be controlled. This can be done by coating the capillary wall with different polymers. The magnitude of EOF can be calculated in terms of velocity, or mobility, as:-

(1.6) $$\nu_{eof} = \frac{\varepsilon\zeta}{\eta} E \quad \text{or} \quad \mu_{eof} = \frac{\varepsilon\zeta}{\eta}$$

Where, ν_{eof} is the electro-osmotic flow velocity and μ_{EOF} is the electrophoretic mobility. 'ε' is the dielectric constant and 'ζ' is the zeta potential. This zeta potential is important in determining velocity of EOF[19]. The zeta potential is pH dependent. At high pH Silanol groups are deprotonated resulting in high EOF, while at low pH Silanol groups are protonated resulting in low EOF due to reduced zeta potential. Thus, at high pH, EOF is fast resulting in poor separation. Likewise, if EOF is very slow diffusion occurs, resulting in band broadening and longer analysis time. Thus, EOF needs to be controlled and optimized. The most important property of EOF is the flat flow profile. Since the flow is uniform along the capillary, there is no pressure drop within the capillary. This uniform plug like flow is one of the advantages of CE as it reduces the dispersion of solutes and band broadening as compared to pressure driven flow.

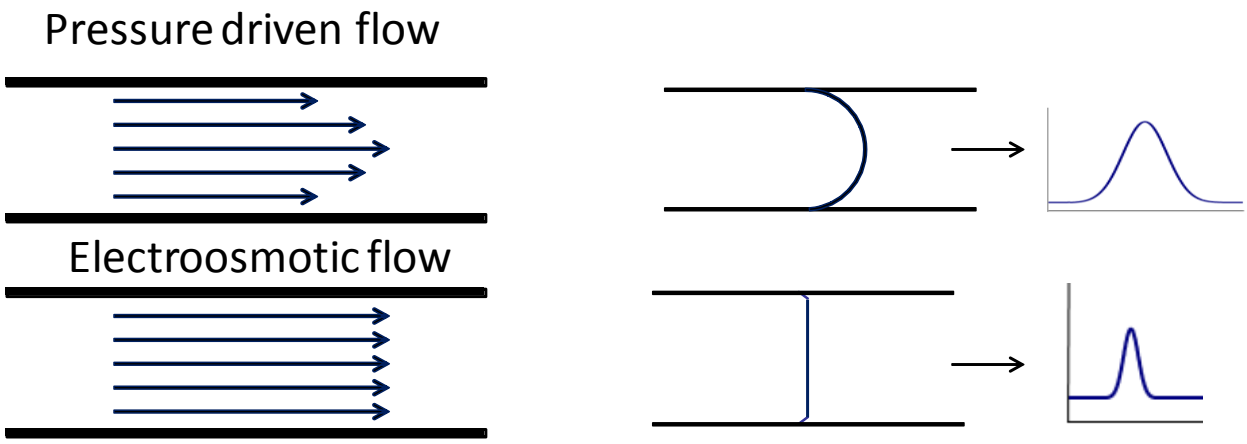

Figure 1-2: Velocity profile for pressure driven and electrokinetic flow through a capillary.

The electro-osmotic velocity of the bulk liquid can be described by the Smoluchowski equation[20]:

(1.7) $$\nu_{eof} = \frac{kE}{\eta}\varepsilon_o = \mu_{eo} E$$

Where, ε_0 is the permittivity of the free space, k is the dielectric constant and μ_{eo} is the electroosmotic mobility. Therefore, total velocity or electrokinetic velocity of an analyte is given as-

(1.8) $$\nu_{ek} = (\mu_{eo} + \mu_{ep})E$$

An advantage of CE is that $\mu_{eo} > \mu_{ep\ anion}$, therefore, all analytes have an overall migration toward the cathode and detector.

1.3. Instrumentation of CE

Capillary electrophoresis is carried out with simple instrumentation, consisting of a silica capillary, two buffer vials, one sample vial , power supply, and the detector. The capillary is

usually about 25-100 cm long with internal diameter of 50-300 microns. The two ends of the capillary are immersed in buffers and an electric field of about 30kV is applied between them. The electrolyte is normally a salt with different pH and ionic strength and it is filtered and degassed before use. Sometimes this electrolyte solution contains additives like surfactants and organic modifiers that help generate better separations.

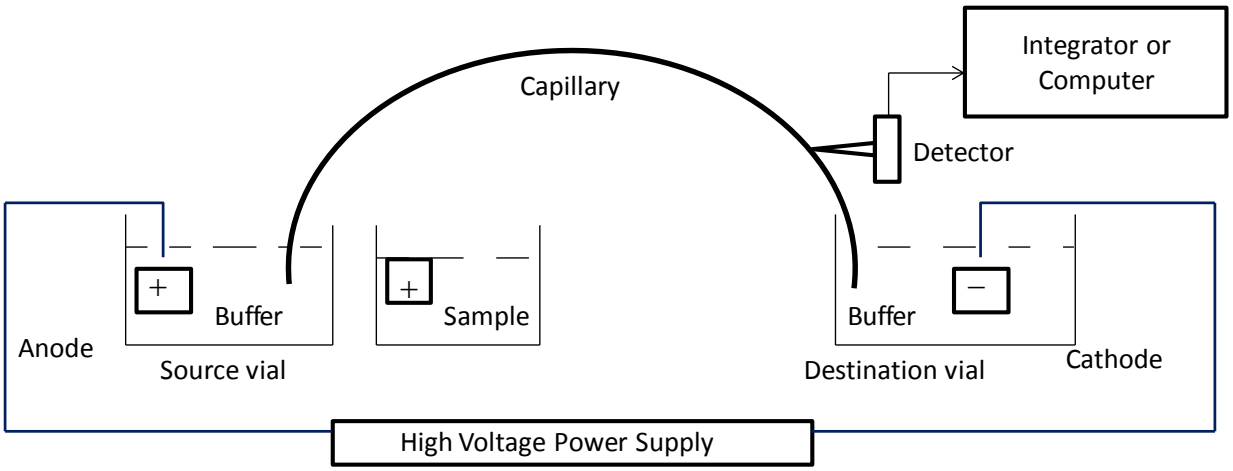

Figure 1-3: A simple setup for Capillary Electrophoresis.

A high voltage power supply is used to generate the desired electric field . Most of the time CE is interfaced with UV-Vis detectors or mass spectrometers. There are two different methods of introducing sample to the capillary. Hydrodynamic Injection is performed by applying pressure or vacuum to one end of the capillary. Due to the pressure difference between the two ends, liquid flows from one end to the other. Electrokinetic Injection is done by applying voltage at one end while the other end is grounded. Due to this voltage difference, ions move from the tip of the capillary to the other end.

The movement of ions is further illustrated in the following figure:

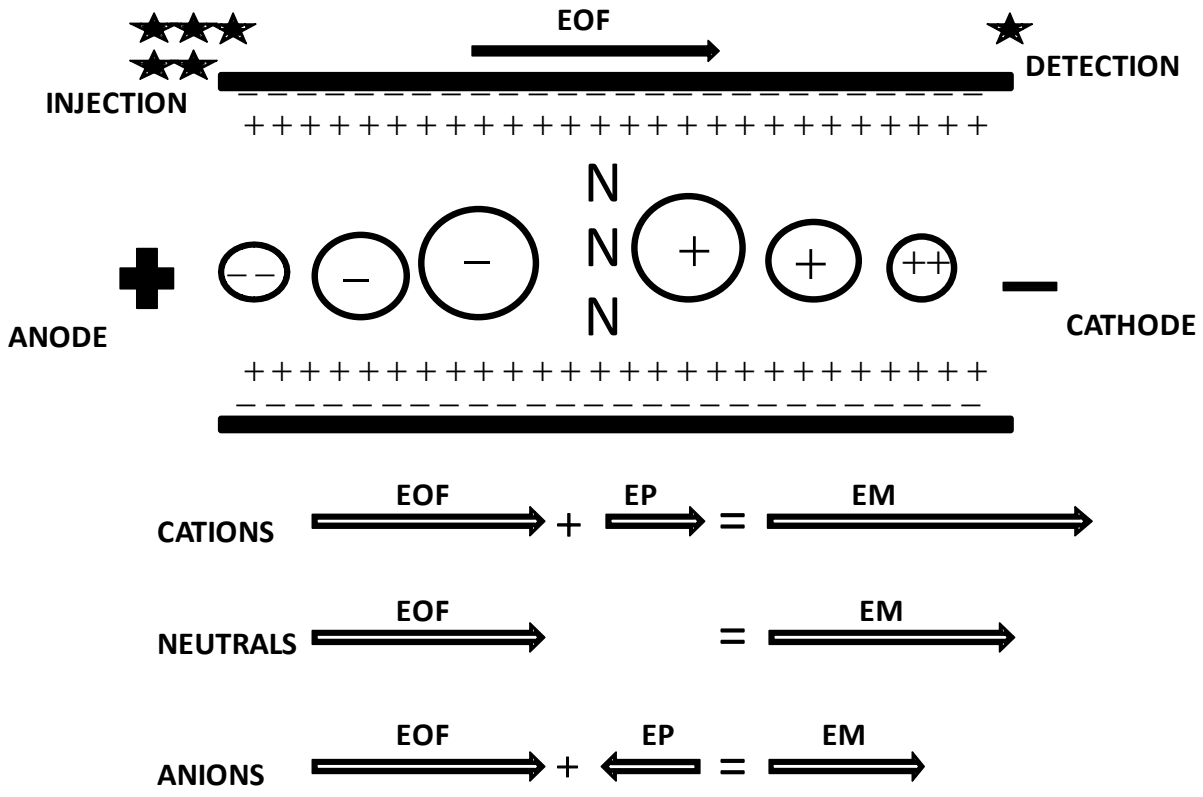

Figure 1-4: Movement of differently charged ions under electric field during capillary electrophoresis.

When the electric field is applied cations migrate toward the cathode, along with the electroosmotic velocity and their own electrophoretic velocity, thus moving faster. Anions, on the other hand, try to migrate toward the anode. Yet, the electroosmotic velocity is larger than its electrophoretic velocity, therefore net movement will be toward the cathode, thus moving slower. Neutral analytes, given that they do not possess charge, move with the electroosmotic velocity. Consequently, the analytes are separated and detected.

1.3.1 Separation Parameters

In electrophoretic separations, the sample is injected at one end of the column and an electropherogram is recorded as analytes pass through the detection window that is situated at a certain desired distance in the separation channel. Electropherograms are recorded as changes in signal intensity from the detector as a function of time (Figure 1-5).

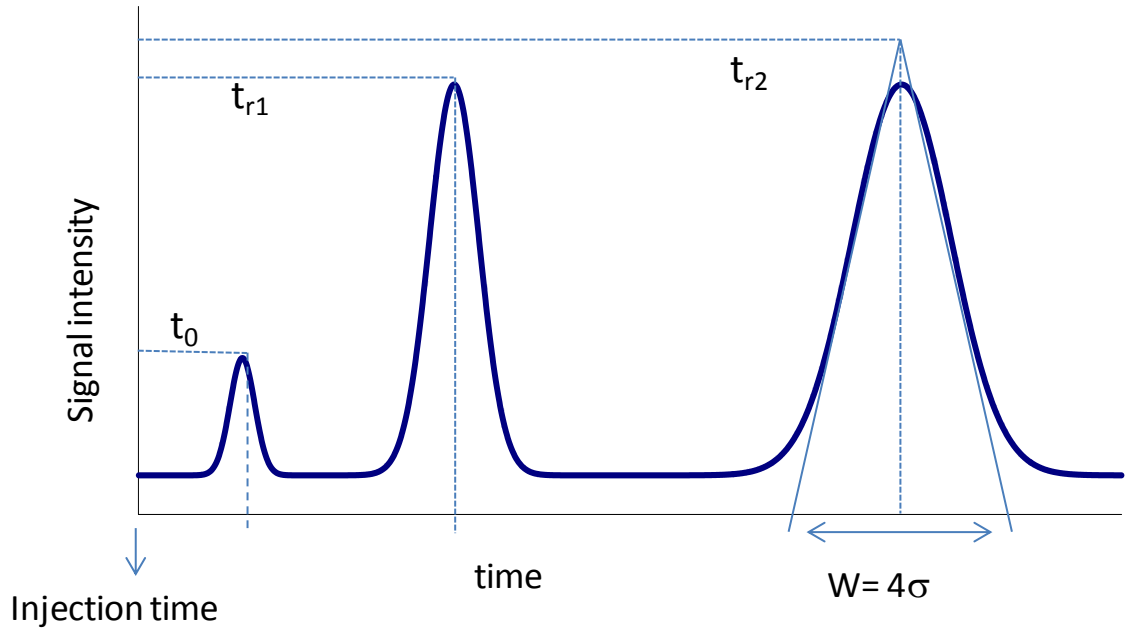

Figure 1-5: Electropherogram showing different analytical parameters, where (t_0) is the migration time of an early eluting species, (t_{r1}) is the migration time for first eluted species while (t_{r2}) is the migration time for late eluting species. The width of a peak is equal to four time its variance.

During the course of separation, solute molecules tend to spread out in all directions. This spreading of analyte band, or band broadening, is largely due to stochastic processes. As a result, when the solute band is seen as a peak in an electropherogram, it will have a Gaussian profile.

The analyte band width, also called baseline peak width (w), is described in terms of standard deviation of the Gaussian shape, where:

(1.9) $$w = 4\sigma$$

If the only source of dispersion is diffusion then the variance, σ^2, can be defined as:

(1.10) $$\sigma^2 = 2Dt$$

Substituting t=L/u into equation (1.10), the variance will be equal to:

(1.11) $$\sigma^2 = \frac{2DL}{u}$$

Where D is the diffusion coefficient of the analytes, t is the migration time, and u is the velocity of the analyte molecule. So, the smaller the value of variance the lesser the dispersion. There are different sources of band broadening, such as diffusion (*diff*), injection (*inj*), detection (*det*), Joule heating (*joule*), parabolic flow (*flow*), channel geometry (*geo*), mass transfer effects (*mt*), electrodispersion (*edisp*), and molecular adsorption (*ads*) that lead to an increase in variance. Thus, the total variance can be defined as the sum of each factor:

(1.12) $$\boldsymbol{\sigma^2_{total}} = \boldsymbol{\sigma^2_{diff}} + \boldsymbol{\sigma^2_{inj}} + \boldsymbol{\sigma^2_{det}} + \boldsymbol{\sigma^2_{edisp}} + \boldsymbol{\sigma^2_{joule}} + \boldsymbol{\sigma^2_{flow}} + \boldsymbol{\sigma^2_{geo}} + \boldsymbol{\sigma^2_{\mathrm{mt}}} + + \boldsymbol{\sigma^2_{ads}}$$

All of these sources except diffusion are negligible most of the time and therefore can generally be ignored. Electrodispersion arises when there are large differences in the ionic strength of the sample and buffer. This can be controlled if the sample concentration is kept at least three orders of magnitude lower than that of the buffer. Joule heating arises due to the heat generated by the passage of electrical current. Joule heating depends on power generated and is also minor until

the field strength is below 1W/cm. Parabolic flow, which arises from different height of liquid in the reservoirs, can be minimised by keeping the height of the solution constant.

There are a number of parameters that are used to determine the quality of separation or separation efficiency. Separation efficiency can be numerically estimated in terms of plate height (H) and plate number (N).

Variance per unit separation length (L) is called plate height (H) which can be given as:

(1.13) $$H = \frac{\sigma^2}{L}$$

Combining equations (1.11) and (1.13) gives:

(1.14) $$H = \frac{2D}{u}$$

This simple expression for plate height does not consider all types of band broadening that occur in a separation. The van-Deemter equation gives a more descriptive form:

(1.15) $$H = A + \frac{B}{u} + Cu$$

Where A is the Eddy diffusion term, which in the case of CE does not exist since there is no packing. B/u is due to longitudinal diffusion and Cu due to the mass transfer between the stationary and mobile phases, which again, in terms of CE, does not exist.

The number of theoretical plates, N, is related to the plate height by:

(1.16) $$\mathrm{N} = \frac{\mathrm{L}}{\mathrm{H}} = \left[\frac{\mathrm{L}}{\sigma}\right]^2$$

Separation with a large number of theoretical plates is considered a good separation. Accordingly, from the above expression we can see that a smaller value of plate height and variance increases separation efficiency, while increasing the separation length increases it.

Another important factor used to determine the quality of a separation is resolution(R_s). Resolution is measure of the between two peaks. It is defined as the distance between the centers of two consecutive peaks divided by their average width and given mathematically as:

(1.17) $$R_s = \frac{2(t2-t1)}{(w1+w2)} = \frac{\Delta t}{4\sigma}$$

Where t_2 and t_1 are the migration times for peaks 1 and 2, respectively, and w_1 and w_2 are the peak widths. A resolution of 1.5 indicates that the peaks are base line resolved.

1.4 Ultraviolet Absorption Spectroscopy

Absorption spectroscopy allows determination of different organic, biological, and inorganic species quantitatively. Molecular absorption study in the ultraviolet (UV), infrared and visible range are mostly used in today's research. UV range refers to the wavelength of light ranging from 200nm to 400nm. Absorption of ultraviolet radiation results in the excitation of a molecule from its ground state to excited state. The absorbance or transmittance of UV light by a species is based on the molecular absorption. When monochromatic radiation passes through a particular solution of interest contained in a cell having a certain path length, according to Beer's law the absorbance (A) of an absorbing species is directly related to the concentration (C) :

(1.18) $$A = \varepsilon\, b\, C = -\log T = \log \frac{I_0}{I}$$

Where, ε is molar extinction coefficient of absorbing species, b is path length of sample and C is concentration of absorbing species. 'T' is the transmittance, 'I_0' is the intensity of incident light

and ‘I’ is the intensity after it passes through the sample[21,22]. Therefore, at a fixed path length concentration of an absorbing species can be calculated from its absorbance.

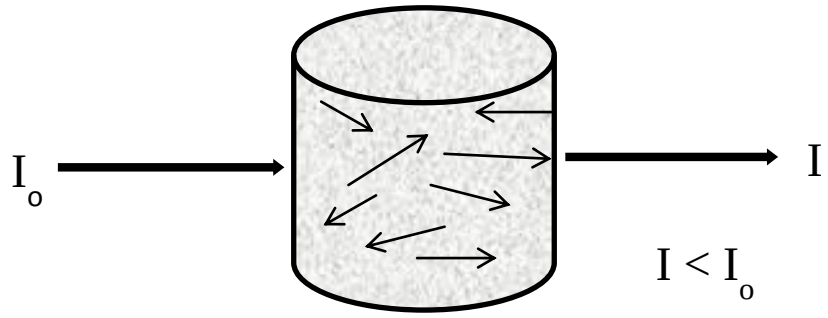

Figure 1-6: Intensity loss due to scattering and absorption.

Deviations from Beer’s law occur in different cases. Beer’s law describes absorption behavior at low analyte concentrations. So, as we increase concentration, the extent of solute-solvent interactions and solute-solute interactions will affect the absorptivity of an analyte. This will finally affect the absorbance.

1.4.1 How Does a UV Spectrometer Work?

A UV spectrometer consists of various parts, such as a monochromator, light source, sample cell, detector, amplifier, and an integrator or computer.

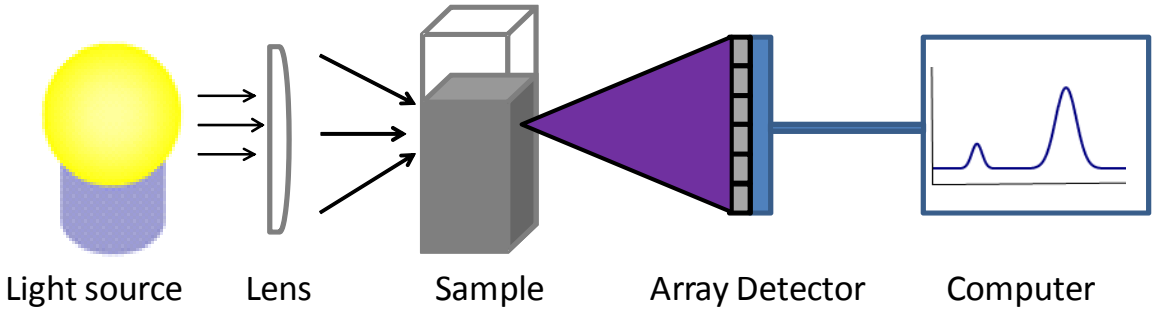

Figure 1-7: UV Spectrometer in our lab.

A continuum light source is necessary that yields a constant intensity and low noise over long periods of time. Among different light sources, Hydrogen and Deuterium lamps are most commonly used as UV source. The sample cell is generally a cuvette or a holder that is made of material that passes the radiation in the spectral region of interest. The detector consists of simply photodiode arrays which collects light from the sample. In our case, it is a charged coupled detector (ccd). The data are recorded in a computer that is connected to the detector. In many instances, detection is affected by instrumental noise due to stray/scattered radiations. In all spectrophotometers, a wide range of wavelengths of light enters the polychromator from the sources, but only a narrow band exits. So inside the polychromator, scattering and diffraction of light occur thus, giving rise to stray light. Stray light or false light is the amount of light measured that is outside the bandwidth of the selected wavelength. Stray light results in a decrease in absorbance. It also affects the linearity of the calibration curve, thus decreasing the linear working range of the instrument. In absence of stray light, absorbance can be simply calculated from equation 1.18. But in presence of stray light, it becomes:

(1.19) $$A = \log \frac{I_0 + I_s}{I + I_s}$$

Where $I_{s,}$ is the intensity of the stray light.

1.4.2 Absorbance Detection in CE Systems

A number of detection methods are available for CE separation systems that include absorbance detection, amperometry, conductivity and fluorescence. Among these detection methods, absorbance detection has become the most commonly used for capillary electrophoresis. This is convenient because the majority of samples analyzed absorb within the UV region. Absorbance detection does not require chemical modification of samples prior to analysis such as other detectors do, and it is also simple to use. A number of papers have been published in the past few years regarding absorbance detection in CE. In an absorbance detection system, the sensitivity of the detector depends upon the molar absorptivity of an analyte and the effective path length. One of the major disadvantages of absorbance detection in CE is the short path length, due to the smaller diameter of the capillary. This results in poor limit of detection and detector sensitivity. Subsequently, work on different methods to improve UV-Vis detector sensitivity is currently being explored. Currently, extended path length and sample stacking are very popular. Different designs such as bubble cell and Z-flow cell have been employed to increase the path length. In such designs, a small portion of capillary lumen is expanded to form a bubble shape without increasing the overall capillary area. This results in increased sensitivity while maintaining the same separation efficiency. Another approach to increase sensitivity of absorbance detectors is by sample stacking or the pre-concentration method. This system depends upon the field strength difference between sample zone and background electrolyte (BGE) or buffer zone. When the conductivity of the sample zone is lower than that of BGE zone, voltage application will cause the ions in the sample zone to move faster. But, when they reach the sample/ buffer boundary, field strength decreases and they migrate more slowly. This

continues until all the ions in sample reach the boundary and cause the sample to be concentrated in a small area/zone. At this point, the field becomes homogeneous and normal electrophoresis occurs. However, for wheat proteins detection, UV detection provides adequate sensitivity because we are not limited by sample amount, as gluten proteins are in rather high concentrations[23].

2 Introduction to Microfluidics and Microchip Electrophoresis

Microfluidics has become a popular area of research in the field of analytical chemistry. Other common terms for microfluidic devices are "micro total analysis systems" or "lab-on-a-chip". The designation "micro" refers to the characteristic length scale of the fluid handling architecture which typically lies between 10^{-6} to 10^{-3} meters[24,25]. With such small dimensions, this device generally handles fluid volumes between 10^{-15} and 10^{-9} liters. Microfluidic devices have many advantages over other conventional systems[26,27]. Due to the small channel dimensions and high surface to volume ratio of the channels, thermal transport is faster as compared to capillaries. The small channels also allow for a more efficient use of space, which enables the fabrication of number of parallel systems. The combined effect of these two advantages allows for high throughput analysis compared to conventional chemical analysis instrumentation like CE. These characteristics of microfluidic devices, make it easier to integrate all assay operations (i.e. sample treatment, preparation, separation and detection) onto a single chip[28]. These devices have been utilized for a number of high-profile uses, such as protein separation, medical diagnosis, aircraft engineering, and food quality control to name a few. The typical design consists of multiple intersecting channels on a single substrate. These different channels allows for multiple detection point simultaneously. Most commonly used are straight channel, T-junction, and cross channel designs. In these designs, two different fluids can be brought into contact at an intersection of channels. Due to fluid switching, they can be separated as they move down the separation channels. Using electro-kinetic transport, many samples can be injected at the intersection and separated. Such microfluidics systems have been used in single cell analysis[29,30], cell culture handling[31], protein detection and disease diagnosis. A combination of

Ohm's Law and Kirchhoff's Law is used to calculate the voltage at the intersection of these different channels:

(2.1) $$V = IR$$

(2.2) $$\sum_{k=1}^{n} Ik = 0$$

According to Kirchhoff's Law, the current that passes into an intersection is equal to the current out of the intersection. Using this law voltage at the intersection can be calculated, and thus electric field can be calculated using the voltage drop from the intersection to the end of separation channel, as well as the channel length. Another advantage of these devices is the increased electric field. Since the channel dimensions are very small in such devices, surface area to volume ratio is high, allowing for better heat dissipation. Also, the decrease in length requires a lower voltage to generate a high electric field, and the increased electric field leads to separation in much less time. This reduced separation time can be explained from the following equation:

(2.3) $$t = \frac{l}{\mu E} = \frac{l L}{\mu V}$$

Where t is the migration time, l is the capillary effective length (to the detector), L is the total capillary length, μ is the solute mobility, E is the electric field, and v is the applied voltage. A further advantage of these devices is decreased sample injection, which reduces the initial analyte bandwidth.

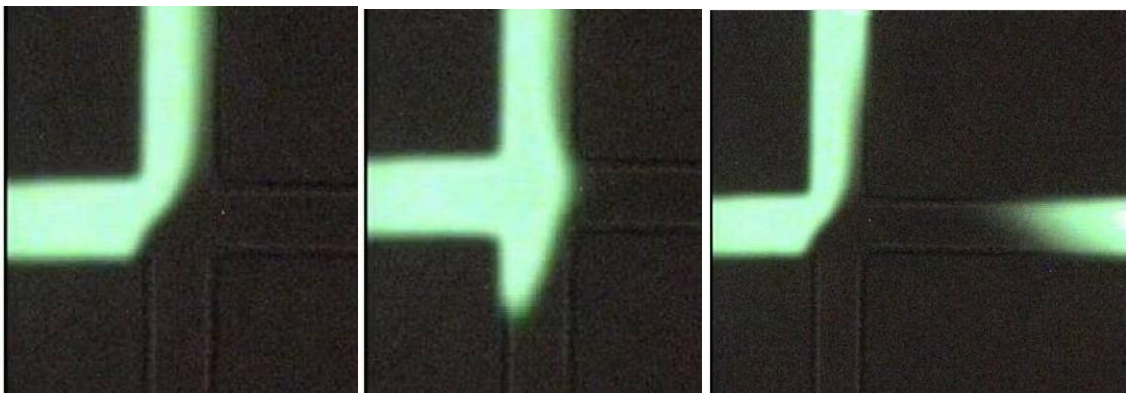

Figure 2-1: Electrokinetic injection scheme in a microfluidic device.

Fluid flow on the macro scale is dominated by inertial forces. However, in the case of microfluidic viscous drag is dominant and causes a reduced flow rate. The relationship between these two forces can be defined by Reynolds number, which is a measure of the flow characteristics of a fluidic stream, given by:

(2.4) $$R_e = \frac{d_c \rho v}{\eta}$$

Where d_c is the length of the channel, ρ is the fluid density, *v* is the fluid velocity and η is the fluid viscosity. At R_e values less than 2300, there is laminar flow giving a parallel fluid flow without either being disturbed[32] . In such a case, mixing occurs by diffusion. But as the inertial forces in the system become greater than 2300, flow will be turbulent and mixing is due to convection. Generally in microfluidics turbulent flow is not desired, as it increases mixing and band broadening. The Reynolds number for fluid flow in microfluidics channels are usually less than 1 where viscous drag dominates, resulting in laminar flow.

2.1 Microchip Fabrication

A miniaturized gas chromatograph made at Stanford University in 1975 was the first microfluidics device reported[33]. The open-tube GC column was made by milling channels in a

silicon wafer. Without using any sophisticated computer program, this process was tedious, time consuming and used very expensive equipment. Because of this, the project was set aside by researchers until the idea of using the technology for integrated circuit boards was adapted for making microfluidics devices. The main technologies used for the fabrication of microfluidics devices are photolithography, soft lithography and wet chemical processing. Different types of materials are used for fabrication such as poly(dimethylsiloxane) (PDMS), glass, quartz, silicon etc. Polymer devices made up of PDMS have gained much popularity due to reduced fabrication cost. PDMS devices are made through soft lithographic molding using a master mold. A silicon wafer with micromachined features as a master for micromolding was used by Effenhauser et.al[34]. Photolithography was used to fabricate a master in a cheaper and faster way by Duffy et.al[35], which is described in the following section 2.1.1.

2.1.1 Photolithography

The basic process of soft lithography starts with an original pattern called "photomask" which contains the desired features of the device. This photomask is copied onto the surface of a substrate by irradiating a photoactive resist. Photoresists are organic polymers that undergo a chemical reaction when exposed to ultraviolet light that result in certain physical and chemical changes. These changes alter its solubility in certain solvents by orders of magnitude in comparison to what it was before exposure. There are two types of photoresist.

Negative photoresist: This type of photoresist undergoes polymerization reaction upon exposure to light. Thus, the part of the photoresist which is exposed to light gets polymerized and the unexposed part remains soluble and is therefore washed off during development. One of the most common negative photoresist used is SU-8.

Positive photoresist: This type of photoresist undergoes a reaction that weakens the polymer network upon exposure to light. Thus, the part exposed to UV light becomes soluble and the unexposed portion gets polymerized.

SU-8 is composed of an epoxy resin (EPON-SU-8) and a triarylium- sulfonium salt photoinitiator dissolved in a solvent-like cyclopentanone or gamma butyrolactone. There are many advantages of using SU-8 in microfluidics device fabrication. SU-8 can be uniformly applied in the films between 0.5 and 240 um thick, has good adhesion to many substrate materials and has very low absorption in the near ultraviolet region.

The process of mold fabrication is depicted in the figure below:

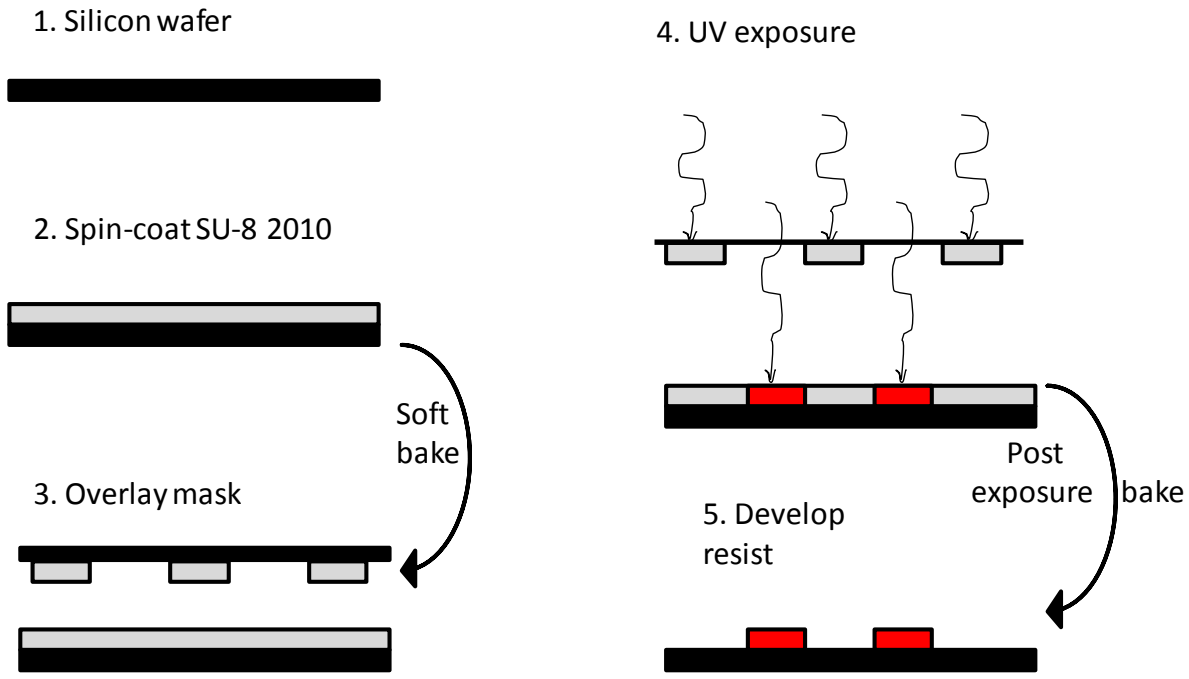

Figure 2-2: Fabrication of a negative tone resist (SU-8 2010) mold using standard photolithography.

For the fabrication of a mold, SU-8 was spincoated on a clean silicon wafer and soft-baked in order to remove the majority of the solvent in the resist and to promote adhesion between the resist and the substrate. After the soft bake, it was exposed under UV light with a photomask on top. The photomask consists of transparent and opaque regions that form a channel pattern. These types of masks were used to make the masks reported in this thesis. There are chrome masks which are fabricated using electron beam lithography. However, this process is expensive and therefore rarely used. A faster and more inexpensive way photomasks can be prepared is by emulsion printing techniques on a plastic transparency films.

Exposure to UV light is performed using a flood exposure system that consists of a mercury arc lamp and optical components. A digital timer is attached that regulates the mechanical shutter in the flood exposure system and determines the magnitude of the radiation dose. This mercury arc lamp emits different wavelengths of UV light: 365nm, 405nm and 436nm also called I, H and G lines, respectively, are common. A long pass filter is used that blocks the transmission of light that is more energetic than 350nm because SU-8 absorbs light strongly below this wavelength. The top part of SU-8 layer is exposed more to light than bottom part. This causes the sidewalls of the structures to have a large inwardly horizontal component to their slope, also called undercut. To avoid this undercut, light is passed through a collimating lens before exposure.

The SU-8 coated substrate was heated again after exposure to complete polymerization. This step is called “post exposure bake”. The substrate was then cooled down to room temperature and placed in a developing bath. The developer selectively removes the unexposed resist and the areas of exposed resist remain as raised structures. This final structure is called a mold. The channel width and height was measured using a surface profiler (Ambios Technology). These molds are used to replicate these dimensions for the channel network on the final PDMS device.

2.1.1.1 Soft Lithography

Soft lithography involves a group of techniques: micro-contact printing, micromolding, and hot embossing in which the features of a structure are replicated in a soft material. Among these, hot embossing and micromolding are used in microfluidics device fabrication. Hard plastics such as polymethylmethacrylate (PMMA) and cyclic olefin copolymer (COC) are generally used for embossing, whereas elastomers such as PDMS are used for molding. Soft lithography has many advantages over other fabrication techniques. First, it is cost effective since it uses polymers that are cheaper than glass and quartz. Second, the use of soft, free-flowing materials allows for structure dimensions on the scale of nanometers to be replicated with ease.

Since the devices presented here are made of PDMS, micromolding is one of the most important techniques used. PDMS is used as a material for microchip fabrication because it is cheap, easy to fabricate, and chemically inert. Also, it can be prepared quickly without the use of any sophisticated instrumentation or clean room facilities, and is optically transparent down to ~230nm. It is also highly suitable for biological applications such as cell culture[36,37,38] and protein detection due to its negligible toxicity and gas permeability. Limitations however include that it swells in organic solvents[39] and shows poor wettability for aqueous solutions.

PDMS is silicon containing organic polymer (Si-O) backbone with methyl groups on the silicon atoms, which are responsible for its flexibility. This special polymer also has a very high level of viscoelasticity due to these loosely entangled flexible polymer chains. The structure is illustrated in the figure below:

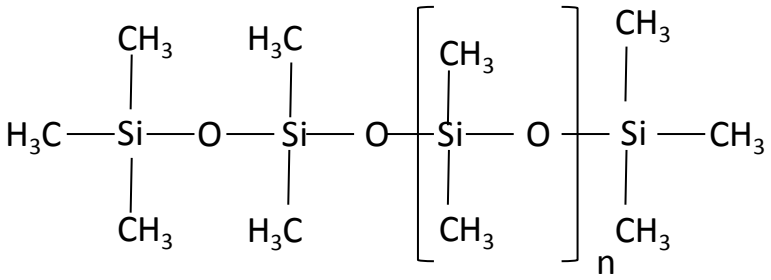

Figure 2-3: The molecular structure of PDMS (Poly (dimethylsiloxane)).

PDMS is a viscous liquid at room temperature. The siloxane bonds give the polymer a great deal of flexibility since functional groups can rotate freely around the center of the bond. For the fabrication of PDMS devices, a commercially available PDMS kit (Dow Corning) is used as a liquid precursor. The methods used by Effenhauser[33] and Duffy[34] employed essentially the same process, which is illustrated in the figure below:

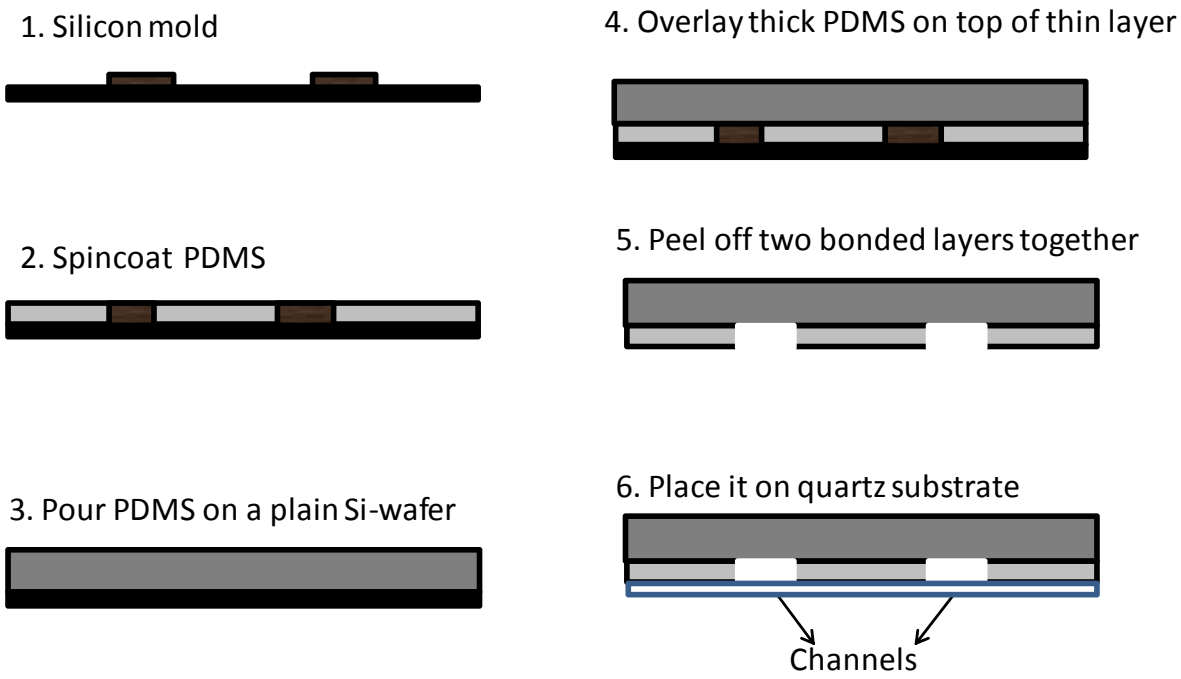

Figure 2-4: Showing the fabrication of a PDMS mold. PDMS precursor is poured on a mold and cured and peeled. This peeled layer is attached to another substrate such that it seals the channels in the PDMS to make a device.

There are two different PDMS precursors that are mixed to form a mold. The dimethylvinyl-terminated dimethyl siloxane precursor acts as the long chain elastomers base, and dimethyl methyl hydride siloxane precursor acts as the short chain cross linker. A 2-carbon linkage between silicon atoms on different precursor molecules is formed when these two precursors are mixed. The degree of crosslinking can be controlled by varying the amount of hydride-containing precursor. The structures of both of these precursors, pre- and post-mixing, are shown in the figure below:

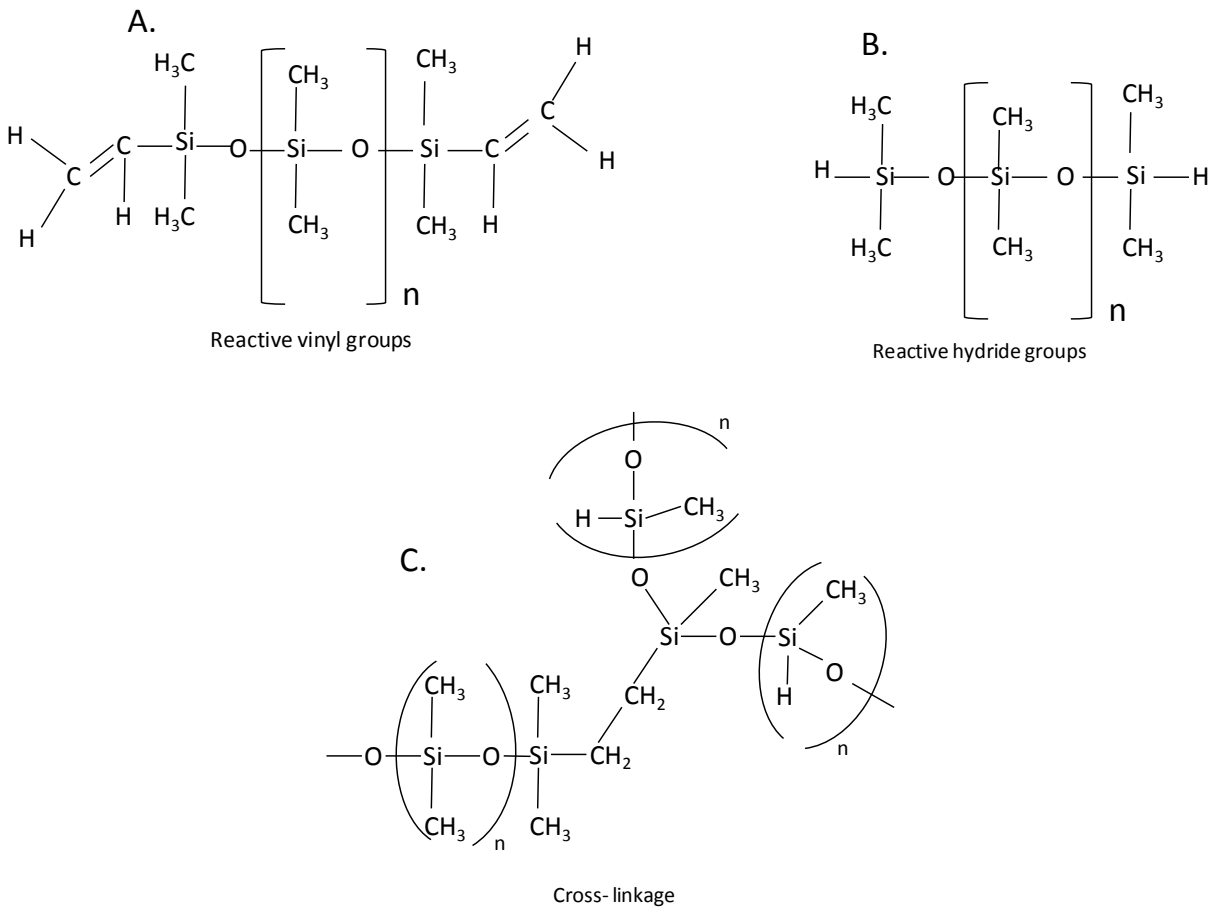

Figure 2-5: The molecular structure of vinyl terminated long chain precursor (A) , hydride terminated short chain cross linker (B) and the structure after they react with each other(C).

Both of these precursors were mixed thoroughly in 10:1 base to curing agent ratios, degassed under vacuum, poured onto a silicon mold and baked in an 80°C oven for one hour. Once cured, PDMS layer is peeled off and bonded to a substrate so that channels in the PDMS were enclosed. Holes were then punched in the reservoir areas to provide fluidic access to the channels. This bond can be either reversible or irreversible. In the reversible case, the advantage is that it can be peeled off, cleaned and reused. In contrast, when it was irreversible it was not reusable.

2.2 UV-Vis Absorbance Detection on a Microfluidics Device

There are different detection techniques such as UV-Vis, Laser Induced Fluorescence (LIF) etc. that can be coupled with CE or microchip CE. Among those, UV-Vis absorbance detection has gained much attention for electrophoretic and micro- level separations. Simplicity, versatility (most organic compounds absorb light in this range), wide applicability, selectivity and commercial availability are some of the reasons for its popularity as a detector. Most analytes have to be derivatized in order to be detected by LIF. This disadvantage of LIF is not present in UV-Vis since analytes do not need any sample derivatization.

The sensitivity of a UV-Vis detector depends on the molar absorptivity of an analyte. This is a measure of an analytes ability to absorb light at a specified wavelength and on the optical path length. For any quantitative analysis, molar absorptivity of at least 10^3 is generally necessary for the analytes to be detected at reasonable concentrations. In absorbance detection in CE and MCE, a short optical path length results in high concentration limit of detection. This accounts for the low sensitivity of UV-Vis detection in a microchip since the channel depth used is very small. Several attempts have been made in the past few years to enhance the sensitivity of absorbance detection by increasing the path length. The use of rectangular capillaries[40], bubble cells[41,42], and z-cells[43,44] are some commonly reported methods. UV-Vis absorbance detection in a microchip has been reported where the optical path length is only tens of micrometers. Recently, a U-shaped detection cell was used by Kutter and his co-workers in an attempt to increase path length. Unfortunately, once again light dispersion was a problem due to stray light effects[45,46].

2.3 Wheat Cultivars

Wheat (*Triticum aestivum*) is one of the most studied cereal foods. The gluten proteins are the major proteins found in wheat endosperm. However, other soluble proteins like albumins and globulins are also present. Cohesive, viscoelastic dough is formed when wheat flour is mixed with water. Wheat is the only cereal that forms such dough. Gluten proteins in wheat are believed to be primarily responsible for that uniqueness. Gluten protein is also responsible for the ability of wheat to retain gas during fermentation and for the rise of bread during baking. The gluten protein in wheat is divided into two sub classes of proteins: gliadins (monomeric form) and glutenins (polymeric form). These two forms can be separated easily because gliadins are soluble in alcohol while glutenins precipitate. Why gluten proteins interact with themselves to form such dough is still unknown. However, it is known that the ratios of these proteins determine the cohesiveness of the dough and also serve as an indicator of the bread making quality of the wheat. The protein content in wheat is determined by the growing environment and the genetics. Generally, gliadin proteins are not affected by environmental factors and thus, have been found as a reliable experimental source for identification. Manipulation of the genetics allows one to control only about 50% of the end use quality of the wheat. Currently, the bread making quality of wheat is determined by actually baking test loaves of bread. But this process is time consuming and wasteful if the wheat is not good for bread. So, the main goal of this project was to create fingerprints of gliadin and gluten proteins for different wheat cultivars as a function of environmental conditions. This would then allow wheat kernels to be analyzed and assessed right after harvest to determine their appropriateness for making bread or pasta or cookies.

3 Experiments

3.1 Chemicals

SU8-2010 was purchased from Sigma Aldrich. 1" by 2" quartz slides were purchased from ESCO Products. PDMS (Sylgard 184 and Sylgard 527 silicone elastomers kits) was obtained from Dow Corning (Midland, MI). Sodium Borate was purchased from Fisher Scientific (Pittsburgh, PA) and Sodium Dodecyl Sulphate (SDS) was obtained from Sigma Chemicals Co. (St.Louis, MO). 2',7'-dichlorofluorescein (DCF) was obtained from Acros Organics(Morris Plains, NJ). All of these chemicals were used as received. Distilled and deionized water purified with an E-pure system (Barnstead, Dubuque, IA) was used to prepare all the solutions necessary for the experiment. All the solutions were filtered through a 0.45mm PVDF filters purchased from Fisher Scientific before introducing in the microfluidics device. The quartz slides were rinsed in Piranha (70% H_2SO_4+ 30% H_2O_2) before using.

3.2 Gliadin wheat protein extraction

10:1 ratio of solvent to flour has been found yielding the best reproducibility results. Thus, gliadins were extracted from 100mg of wheat flour using 1ml of 50% propanol in water in an eppendrof tube as described previously[47,48]. Briefly, 100mg flour was mixed in 1ml 50% propanol and vortexed for 1min and then centrifuged at 1600rpm for 2 min. The supernatant was decanted and filtered using a 0.45um filter syringe and stored at -21°C until use.

3.3 CE Electrophoresis

All separations were carried out in a 50μm fused silica capillary (Polymicro Technologies, Phoenix, AZ) using in house CE setup. The capillary length was kept between 25-30cm. The Capillary electrophoresis system consists of a Unicam 4225 UV Detector (Mississauga, Canada) and a Spellman CZE 1000R power supply (Spellman High Voltage Electronics Corp.; Hauppauge, NY). The samples were injected into the separation channel electrokinetically. An in-house written Labview program was used to control the voltage and collect the signal. Prior to CE separations, each capillary was cleaned using the following steps. First, a 50/50 Sodium Hydroxide and methanol was pushed through the capillary for 15min at flow rate of 10μl per min using a BS-8000 syringe pump (Braintree Scientific, Inc.; Braintree, MA). Then the capillary was rinsed with water, coated with 1% Silane solution and baked in oven for 10 min. Separation buffer for performing wheat gliadin separations using capillary electrophoresis had been previously optimized using commercial instruments[49,50]. From these experiments, a low pH phosphate buffer was chosen for our experiments. The buffer consisted of 50mM sodium phosphate (pH 2.5), 20% acetronitrile, and 0.055 HPMC by volume. Sodium phosphate, HPMC and acetonitrile were acquired from Fisher Scientific (Pittsburgh, PA). Acetonitrile served as a cooling agent and prevented joule heating since sodium phosphate is a high conductivity buffer. HPMC and silane coating was used to prevent protein adsorption to the capillary wall.

3.4 Masks

The masks required to transfer the channels pattern into the device is called as photomasks. These photomasks are produced by a photo plotting process at 40,000 dpi (dots per inch) by Fineline Imaging (Colorado Springs, CO). These masks designs were drawn using the

AutoCAD2006LT software (Thompson Learning, Albany, NY) and then sent for printing to the manufacturer (Fineline Imaging). For the study done here, a mask containing the channel network of two intersecting lines was prepared. The upper two channels were shorter as compared to lower ones (Figure 3-1). These upper two channels are same length of 1cm and lower two channels are 8cm in length from the intersection. The width of the channels are 50 um each. The lower two channels are made such that there is a small curved connection between two straight loops. These small curved are narrower in width than the other channels width. It is designed so as to control the flow of liquid and reduce diffusion of anayte which ultimately reduces band broadening.

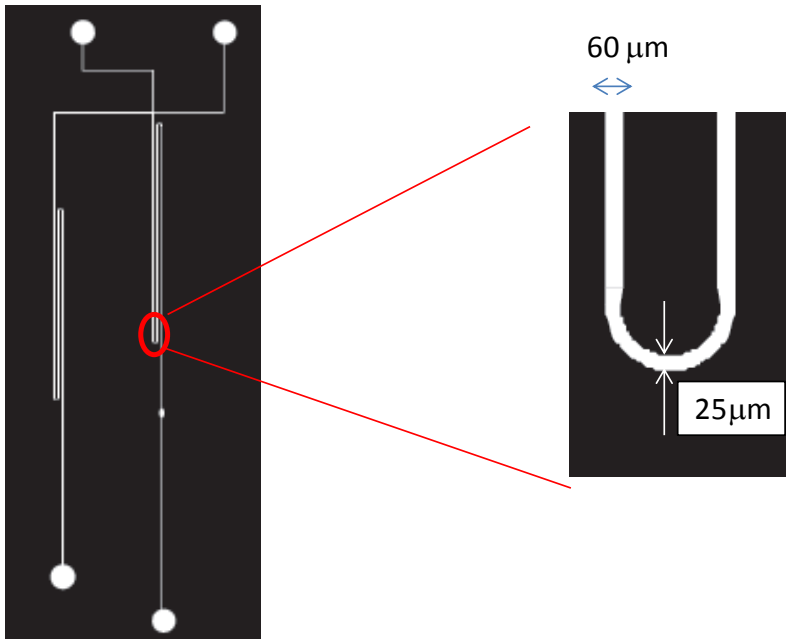

Figure 3-1: Plotted photomask with the channel design.

3.5 SU8 2010 mold fabrication

Based on the previously described methods, a SU8 mold was prepared on a 4" by 4" Silicone wafer (Silicone Inc., Boise, ID). About 4ml of photoresist was applied. This silicon wafer was coated with SU-8 2010, a negative photoresist (Microchem Corp., Newton, MA) using a spincoater (Laurell Technologies, North Wales, PA). The speed at which this photoresist was spun is 1500rpm for 30 seconds. Then, it was incubated at 65°c for 4 minutes then 95 degree for 7 min prior to UV exposure. Then the substrate was exposed to UV exposure dose of ~180mJ/cm^2 using a near-UV flood exposure system (Oriel Instruments) without photomask. The soft bake and hard bake procedure was repeated and photomask placed on the wafer prior to UV exposure. In this case, we had a mask with channels clear and background dark. After UV exposure, background washed off during development and the part in the channel remained. After final baking, it was cooled for 5min and then developed in SU8 developer which is propylene glycol monomethyl ether acetate (PGMEA). It was rinsed with developer and isopropyl alcohol. Then, it was blown dry with liquid Nitrogen. It was inspected under microscope to make sure that all the channels are intact. After this, finally the channel dimensions were measured using a surface profiler from Ambios Technology (Santa Cruz, CA). In this case, this protocol produced a ~ 20um tall SU8 structure which gives same depth to the PDMS channels.

3.6 UV Exposure system

The UV exposure system used in this case is a flood exposure system from Oriel Instruments. It consists of a mercury arc lamp and optical components.

Figure 3-2: Oriel UV- flood exposure system.

3.7 Fabrication of quartz/PDMS microchip

In order to make a PDMS-quartz three layered device, at first a quartz slide was thoroughly cleaned with Piranha solution (70% H_2SO_4 and 30% H_2O_2) for 5 min and then rinsed with deionized water. It was then sonicated in deionized water for 5 min in an Ultrasonic bath. To make PDMS layer, a 20:1(elastomers base to curing agent) mixture was degassed in a vacuum desiccators for 15 min. The bubble free mixture was then poured on a silicon mold containing channel design and spincoated at 1500rpm for 25 sec. This generated a 30 microns thick PDMS layer. After that it was kept in oven for 10 min. Meanwhile, another 10:1 PDMS was also mixed, degassed, and poured on a clean silicon wafer and baked at 80°C for 10min. These two layers were baked simultaneously. After 10 min both of them were removed from the oven and a 1mm pinhole was punched on the thicker PDMS layer using a 1mm biopsy punch. This hole in the thick layer was made to let the UV light pass through our channels because thin layer of PDMS allows UV at 210 nm and thick layer on other parts blocks UV below ~230 nm. Then the thick PDMS was placed on the top of thin PDMS on the Si-mold aligning the hole over the channel.

After this the aligned layers were placed in the oven for another 30 min at 80 °C. Then, PDMS layer was peeled off from the mold making sure that the thin layer came off with the thick layer. The two layers of PDMS were permanently annealed together. The thin layer has the channels on it while thicker layer acts as a support for it. The device was then placed on a quartz slide to seal the channels in the thin layer. Holes were then punched to make the reservoirs. The device was then ready to use and consisted of two PDMS layer and a quartz layer beneath these two layers.

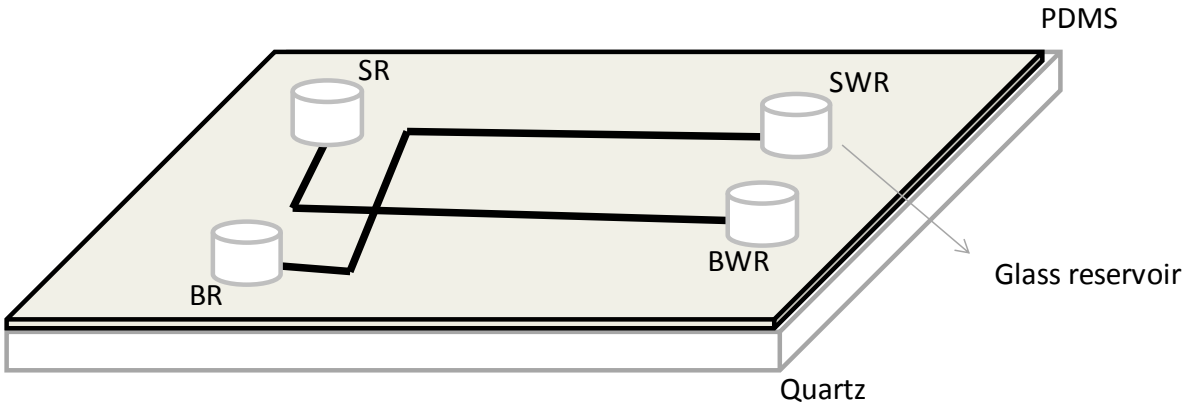

Figure 3-3: Simple diagram for a cross channel microfluidic device. The upper thick and thin layer is made from PDMS and lower layer is a quartz slide. SR = sample reservoir, BR = Buffer reservoir, BWR = buffer waste reservoir and SWR = sample waste reservoir. SR = BR to intersection is 1cm. Intersection to BWR = SWR is 6.5cm.

3.8 Microscopy

At first the device was cleaned with methanol and then filled with water. Then, the device was filled with buffer by adding the buffer solution to the reservoirs and then using a vacuum applied to the end of the separation channel to pull the solution through the channels. To make sure that the device worked, it was checked by filling the analyte reservoir with a buffered 100um fluorescein solution and injections were performed. To perform the injections, the microfluidic device was placed on the stage of a Nikon Eclipse TE2000-U inverted

microscope(Nikon Instruments Inc., Melville, NY) . Voltages were applied to all the four reservoirs using a Bertran high voltage(0-10kV) power supply(Hauppauge, NY). This power supply has 5 separate units that can be controlled by a LabView program software(National Instruments, Austin, TX). High voltage was applied to the upper two reservoirs and lower two were grounded. To record and moitor the injections, a high resolution Sony CCD color video camera was used and the videos were recorded using a Roxio videowave movie creation software. The excitation light was generated using a mercury lamp and a 450-490nm filter block. The channels were observed under 100x magnification using a 10x objective and a 10x transfer lens.

To perform the electrokinetic injection, high voltage was applied to the upper reservoirs- one containing the fluorescein and the other containing a 25mM sodium borate 10mM SDS at pH9. Good injections are shown below:

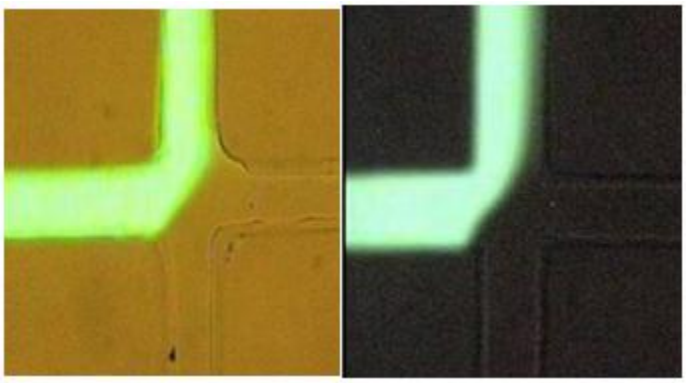

Figure 3-4: Left showing white light image of microfluidic device and right showing fluid flow during a run when voltage is applied.

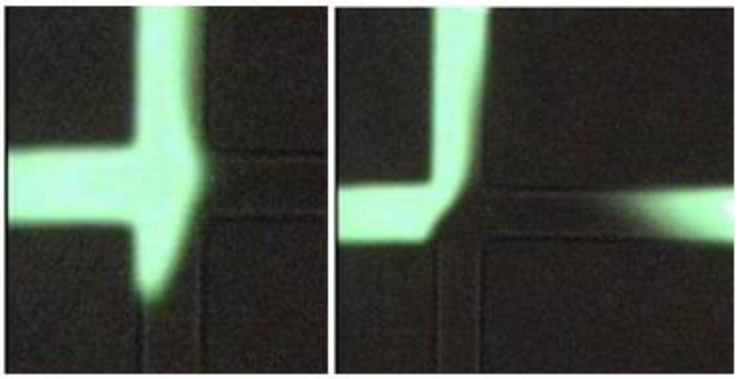

Figure 3-5: Left showing an injection scheme and right showing fluid flow down the separation channel. Channels are 50microns wide.

After confirming that the device was working properly a mixture of aminoacids was tested. A mixture of 3 different aminoacids labeled with Fluorescein Isothiocyanate (FITC) were injected and separated.

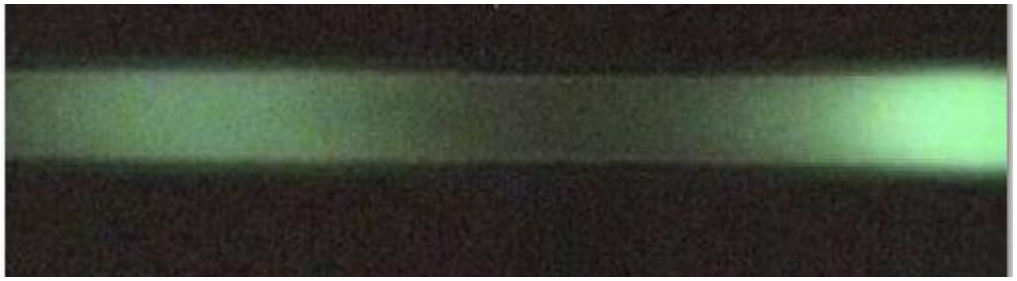

Figure 3-6: Separation of aminoacids as shown two separate bands.

To visualize this separation and collect the data, we made an instrumental setup with a UV detector which is described in detail in section 3.9.

3.9 UV detection Setup

Our detection setup consists of a spectrometer from Ocean Optics with a UV light source. It has a photodiode detector that is aligned right over the detection hole. The setup, as shown in

Figure 1-6, consists of a continuous UV light source, spectrometer, and the microfluidic device. Light is emitted by the source and passes through a collimating lens and at the tip of fiber and then a 12 mm focal length UV transparent lens to focus the light into the microfluidic channel. The microfluidic device has an expanded region (a bubble) in the separation channel that acts as a detection point. The width of the channel in the bubble is about 2-3 times wider than that of the separation channel.

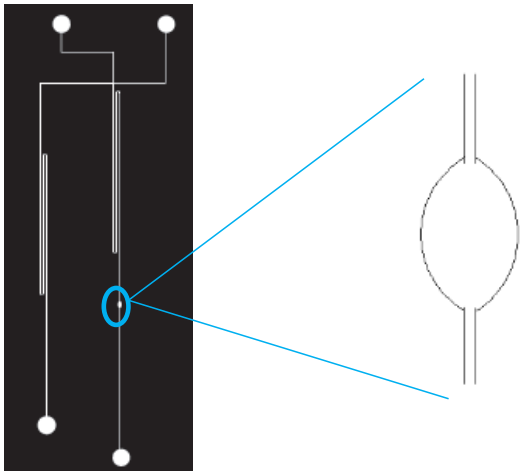

Figure 3-7: Expanded region in our separation channel. The width of channel above and below bubble is 50 μm while at bubble it is 300 μm.

PDMS is optically transparent down to ~230 nm[51]. But decreasing thickness of PDMS layer allows UV light to pass through it. In our case, we used light at 210 nm but our thin PDMS layer of ~30 μm thickness was able to transmit light. The detection point in the device has such thin layer that allows light to pass through it. But all other regions have 2-3 mm pdms on top of this thin layer which cuts off UV below ~230 nm. The spectrometer is controlled with Spectrasuite program and home written Labview program controls the injection system. When the analyte of interest reaches the excitation spot the change in absorption is detected by the detector and visualized as the absorbance verses time plot.

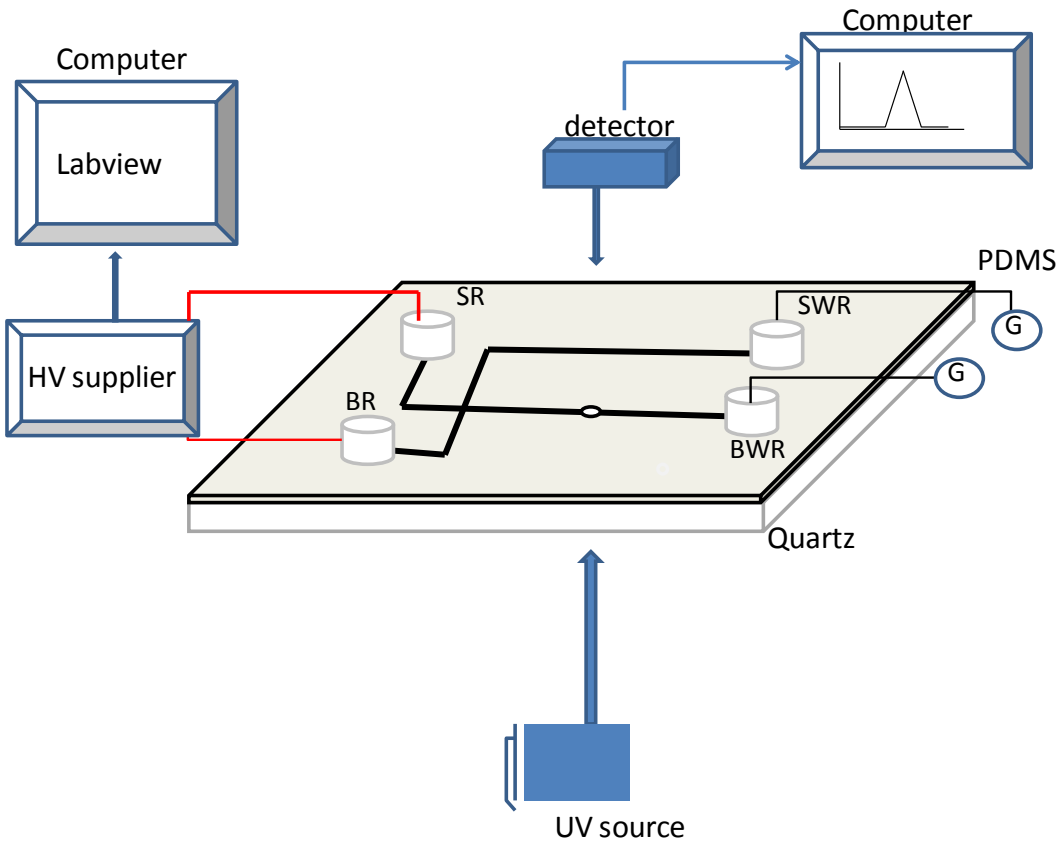

Figure 3-8: UV detection setup designed for microchip electrophoresis. SWR is the sample waste reservoir, BR is the buffer reservoir, SR is the sample reservoir and BWR is the buffer waste reservoir. HV= high voltage and G= ground.

High voltage is applied to the reservoirs using an external high voltage supplier. The voltage in this voltage supplier can be controlled through a Labview program in the computer connected to it. There is a small detection area on our separation channel where UV light can pass. This will act as the cell where sample is loaded. UV light of certain intensity from the source passes through the detection point and then through the sample and fall on a ccd array. The output from the detector array passes to the amplifier and then to a recorder or data acquisition system.

4 Results and Discussions

4.1 CE separation of wheat proteins

The sample containing gliadin proteins of wheat sample were injected electrokinetically into the capillary. It is important that the CE system be capable of performing reproducible separations. Figure 4-1 and 4-2 show the reproducibility for two consecutive injections of Jagger. The reproducibility for the early eluting peak A in Figures 4-1 and 4-2 was less than 1% RSD while for later eluting peak, B in those figure, it was less than 2% RSD.

Table 1: Table showing migration time and the %RSD for the electropherograms obtained.

Figure	Peak	Migration time (sec)	% RSD
4-1	A	227.0	< 1%
4-2	A	230.5	
4-3	A	230.0	
4-1	B	611.0	< 2%
4-2	B	625.0	
4-3	B	635.0	

This is significant because these electropherograms were taken over ~30-40 minutes. These sets of separations demonstrate that the system is capable of maintaining excellent run to run reproducibility over time.

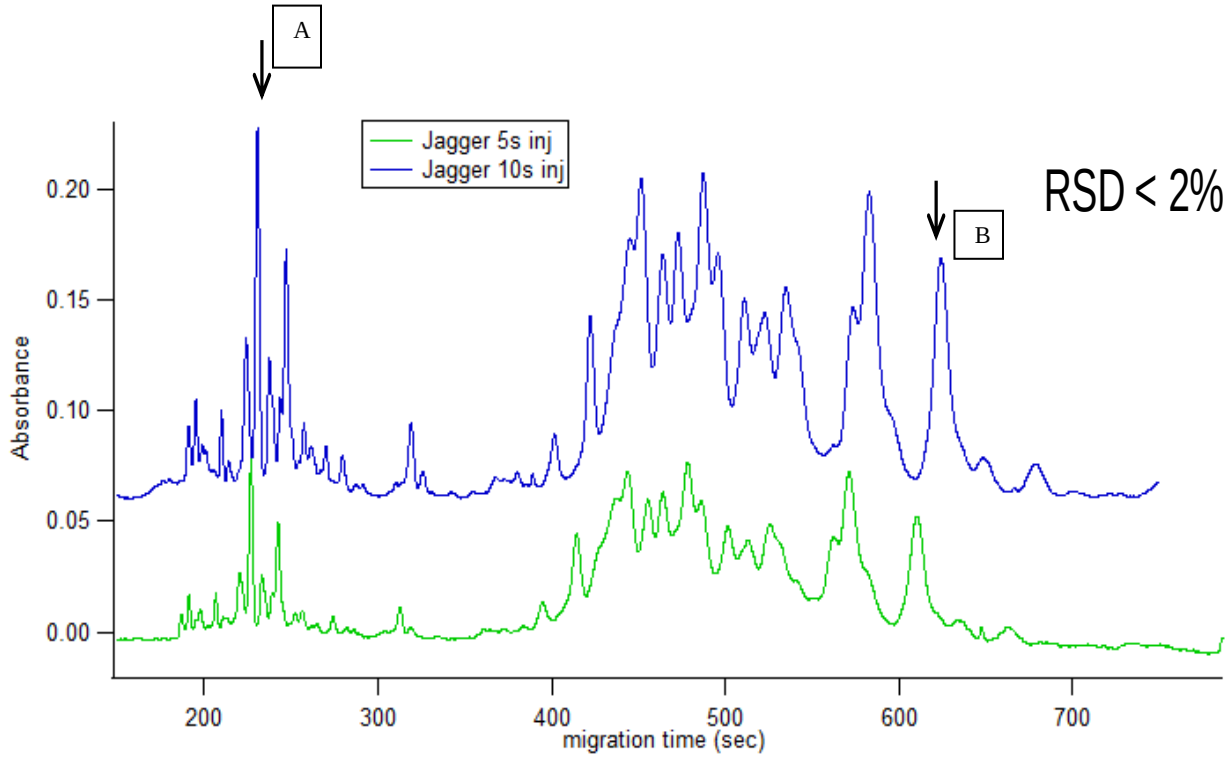

Figure 4-1: Absorption spectra of Jagger wheat protein at 210 nm.

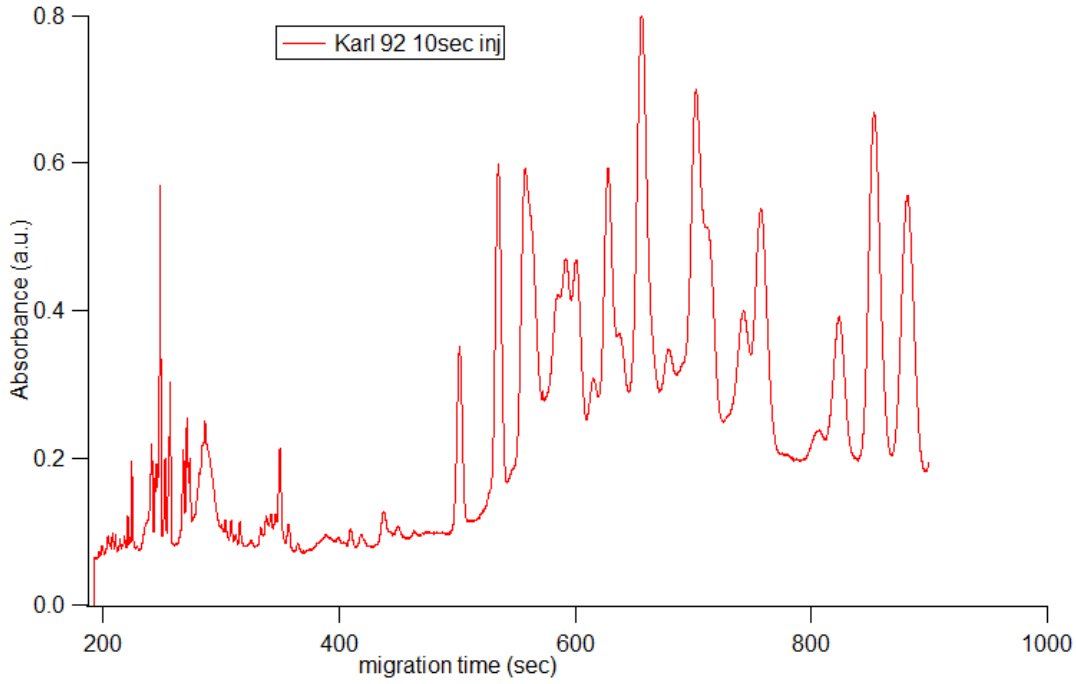

Figure 4-2: Absorbance verses time plot of Karl wheat variety at 210 nm.

Figure 4-2 shows the separation of the Karl92 wheat variety. The peak fingerprint is significantly different from the peak fingerprint for the Jagger variety. A comparison of the 2 separations indicates that the different varieties of closely related wheat cultivars can be differentiated using capillary electrophoresis. The buffer containing 50mM Sodium Phosphate (pH 2.5) with 0.05% HPMC, and 20% acetonitrile worked. The optimized buffer and separation conditions for the capillary will be used as starting point for future separations using a microfluidic device once the UV detection setup is optimized.

4.2 Toward the Separation of Wheat Proteins in Microfluidic Devices Using UV Detection

In previous chapter the construction and testing of microfluidic devices were described. In this chapter the separation efficiency of a microfluidic device integrated with a uv detector is characterized and the limitations of the present setup are described.

To check the separation performance of the device an analyte solution that consists of equimolar mixture of three different amino acids (phenylalanine, tryptophan and glutamic acid 0.25mM) was chosen. The absorption versus time plot of the analyte solution at injection plug length of 40 sec is shown in Figure 4-3 and 4-4.

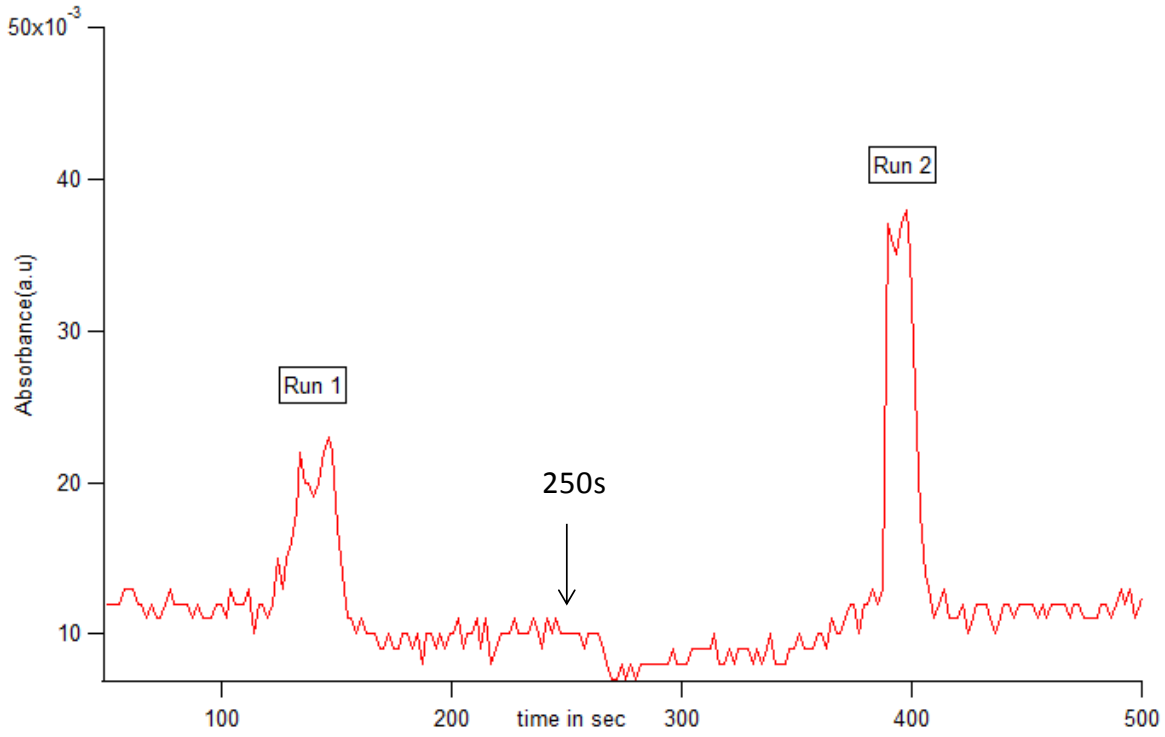

Figure 4-3: Absorbance verses time plot of aminoacids mixture. Arrow represents the start of second run.

Figure 4-3 contains electropherograms from two different runs. From the plot, we can see the separation between two aminoacids but they are not well resolved. It can be related to the low data acquisition rate of the spectrometer.

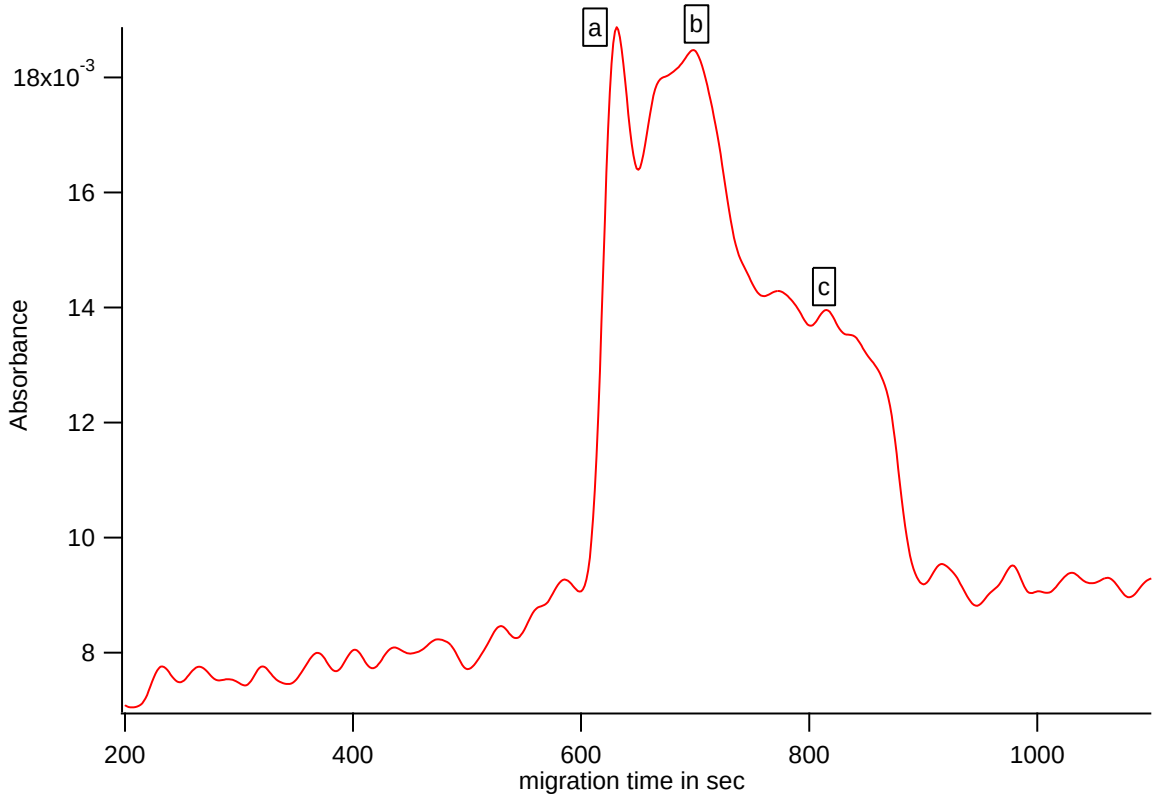

Figure 4-4: Absorbance verses time plot showing separation of aminoacids mixture.

Under ideal conditions i.e. with proper voltage and appropriate concentration and pH of the buffer three well separated peaks are expected. Although three distinct peaks are not seen in the figure, it is significant that three features a, b, and c that probably correspond to three amino acids are observed at ~400, 450, and 550 sec respectively after injection at 200 sec. The ultimate goal for this project is to lower the injection plug length by a factor ~20 and detection time by factor of ~2 so that small volumes of wheat protein samples can be analyzed as quickly as possible.

Before experiments can be run on real samples (wheat protein) the following experimental variables will need to be optimized:

1) Alignment of detector with the device, 2) data acquisition rate (DAQ) of the detector, 3) injection plug length, and 4) the composition of the buffer

The first step is to optimize is the alignment of the detector with the detection point in our device and the light source. Improper alignment results a low light flux into the channel and the presence of stray light. If stray light is high, the signal of our sample will be low and noise will be high.

The second step is to improve the data acquisition rate of the detector. This is critical to be able to optically resolve narrow peaks that are close together. In figures 4-3 and 4-4 the DAQ rate, which is the number of scans/cycles per sec was only 0.6Hz. The effect of DAQ rate on resolution and shape of a peak can be seen from figure 4-5.

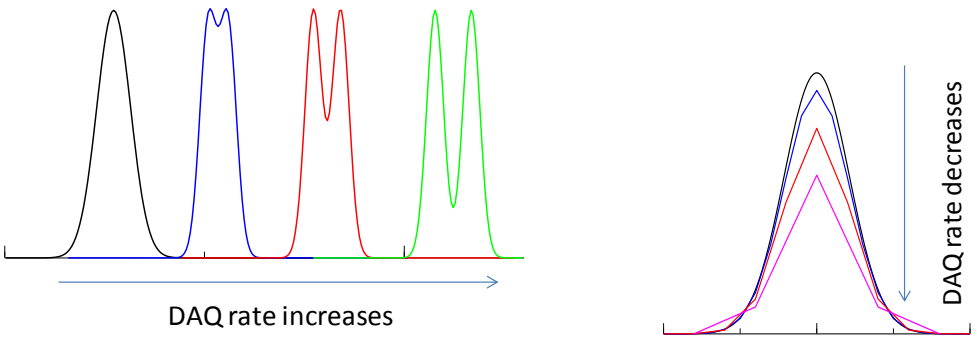

Figure 4-5: Effect of Low DAQ on resolution of a separation. Resolution and peak shape improves as DAQ rate increases.

It might have been one of our problems. In figure 4-3 and 4-4, our peaks are not separated. So, the data acquisition frequency needs to be increased from 20 to 100 fold.

The third step is to optimize the injection plug. We need to perform as short an injection as we can and be able to detect it. Larger injection plug results in higher variance and band broadening/dispersion. The number of theoretical plates which defines the separation efficiency

is inversely proportional to variance square and thus will be low. The proper injection length that will allow the detection of the analytes without substantially decreasing the separation efficiency needs to be determined. The injection may also be using a sample stacking technique. Stacking will occur when the conductivity of sample and buffer is different. This difference in conductivity can be achieved by preparing sample in low concentration buffer than the separation buffer. Using sample stacking an increase of factor of 10 was seen in detectability by Lauer's group[52].

Lastly, the buffer composition needs to be further improved. High buffer concentrations generate high currents and decrease the EOF and zeta potential resulting in longer migration times. Low buffer concentrations may result in sample adsorption. If the conductivity of sample and buffer is different, then distortion of peaks may occur. Likewise, buffer pH is an important factor in determining the velocity of EOF. Low pH buffers will protonate the wall resulting in low EOF. Similarly, high pH buffers will de-protonate the channel wall resulting in very high EOF. This high EOF can cause the elution of the protein bands before separation, while low EOF will result in adsorption of sample to the wall. Protein adsorption can be decreased by coating the channel wall to modify the surface of the channel. Many different coating techniques using nonionic surfactants[53,54] or covalent coatings[55] have been reported.

5 Conclusions

For the UV setup prepared for this work, the ocean optics DAQ rate was not fast enough to allow adequate optical resolution of the peaks. Future work, therefore, will focus on a UV system capable of a higher DAQ rate.

References

1 Osborne, T.B. The proteins of the wheat kernel; Carnegie Institution of Washington: Washington, D.C., **1907**.

2 Jones, B.L.; Lookhart, G.L.; Hall, S.B.; Finney, K.F. *Cereal Chemistry*, **1982**, *59*, 181-188.

3 Sia, S.K.; Whitesides, G.M. Electrophoresis, **2003**, *24*, 3563-3576.

4 Michaelis, L. Electric transport of ferments. (1) *Invertin Biochem, Z.* **1909**, *16*, 81.

5 Tiselius, A. *Trans. Faraday Soc*. **1937**, *33*, 524-531.

6 Dale, G., and Latner, A. L., Isoelectric focusing of serum proteins in a polyacrylamide gels followed by electrophoresis, *Clin. Chem. Acta*, **1969**, *24*, 61.

7 Macko, V., and Stegemann , H. Mapping of potato proteins by combined electro-focusing and electrophoresis. Identification of varieties, Hoppe- Seyler's *Z. Physiol. Chem*., **1969**, *350*, 917.

8 Ishii, J. A study of high performance liquid chromatography. I. Development of technique for miniaturization of high performance liquid chromatography, *J.Chromatogr*., **1978**, *144*, 157.

9 Schomburg, G. Problems and achievements in the instrumentation and column technology for chromatography and capillary electrophoresis, *Chromatographia*, **1990,** *30*, 500.

10 Hjerten, S. High Performance Electrophoresis, *Chromatogr Rev*. **1967,** *9*, 122.

11 Mikkers, F.E.P.; Everaerts, F.M.; Verheggen, Th.P.E.M. *J. Chromatogr*., **1979,** *169*, 11.

12 Jorgenson, J.W.; Lukacs, K.D. Clinical Chemistry. **1981**, *27*, 1551-1553.

13 CE Part I: Theoretical and experimental background. *J.Chem.Ed.Chem.wisc.edu*, **1998,** *75*.

14 Grossman, P.D. and Colburn, J.C., Eds., Capillary electrophoresis: Theory and Practice. New York: Academic Press, **1992**.

15 Li, S.F.Y. Capillary electrophoresis: Principles, Practice and Applications, Elseiver Science, Publishers B.V. Amsterdam, **1992**.

16 Landers, J.P. Eds., Handbook of Capillary Electrophoresis, CRC Press, Boca Raton, **1993**.

17 Helmholtz, H.Z. About electrical interfaces (translated title), *Annal. Phys. Chem*., **1879,** *7*, 337.

18 Hunter, R.J**.** Zeta Potential In Colloid Science: Principles and Applications, Academic Press, UK, **1988**.

19 Schwer, C. and Kenndler, E. Electrophoresis in fused silica capillaries: The influence of organic solvents on the electro-osmotic velocity and the ζ potential, *Anal. Chem*. **1991,** 63.

20 von Smoluchowski, M. *Bull. Int. Aced. Sci*. **1903,** 184.

21 Skoog, D.A.; Holler, F.; Crouch, S.R. Principles of Instrumental analysis, **2007**.

22 Strong, F.C. *Anal. Chem*., **1952,** *24*, 338.

23 Lookhart and Bean. *Cereal chemistry*, **1998**, 374-379.

24 Effenhauser, C.S. In separation Methods in Microanalytical Systems; Kutter, J.P.; Fintschenko, Y., Eds.; CRC Press: Boca Raton, **2006**, 575.

25 Nyugen, N.T.; Wereley, S.T. Fundamentals and Applications of Microfluidics, Artech House, Inc, Boston, **2006**.

26 Harrison, D.J.; Fluri, K.; Seiler, K.; Fan, Z.; Effenhauser, C.S.; Manz, A. *Science*, **1993,** *261*, 895-897.

27 Manz, A.; Graber, N.; Widmer, H.M. *Sens. Actuators. B. Chem*. 1, **1990,** 244-248.

28 Skoog, D.A., West, D.M., Holler, F.J., Fundamentals of Analytical Chemistry, 7ed, Saunders College Publishing, Philadelphia, **1996**.

29 He, M.; Edgar, J.S.; Jeffries, G.D.M.; Lorenz, R.M.; Shelby, J.P. Chiu, D.T. *Anal. Chem*. **2005,** *77*, 1539-1544.

30 McClain, M.A.; Culbertson, C.T.; Jacobson, S.C.; Allbritton, N.L.; Sims, C.E.; Ramsey, J.M. *Anal. Chem*., **2003,** *75*, 5646-5655.

31 Fu, A.Y.; Chou, H.P.; Spence, C.; Arnold, F.H.; Quake, S.R. *Anal. Chem*., **2002,** *74*, 2451-2457.

32 Beebe, D.J.; Mensing, G.A.; Walker, G.M. *Annu. Rev. Biomed. Eng*. **2002,** *4*, 261-286.

33 Terry, S.C.; Jerman, J.H.; Angell, J.B. *IEEE Trans. Electron Devices*, **1979,** *26*, 1880-1886.

34 Effenhauser, C.S.; Bruin, G.J.M.; Paulus, A.; Ehrat, M. *Anal. Chem*. **1997,** *69*, 3451-3457.

35 Duffy, D.C.; McDonald, J.C.; Schueller, O.J.A.; Whitesides, G.M., *Anal. Chem*. **1998,** *70*, 4974-4984.

36 Gu, W.; Zhu, X.; Futai, N.; Cho, B.S.; Takayama, S. *Proc. Natl. Acad. Sci*. USA, **2004,** *101*, 15861-15866.

37 Hung, P.J.; Lee, P.J.; Sabounchii, P.; Aghdam, N.; Lin, R.; Lee, L.P. *Lab Chip*, **2005**, *5*, 44-48 .

38 Rhee, S.W.; Taylor, A.M.; Tu, C.H.; Cribbs, D.H.; C.W., Jeon, N.L. *Lab Chip*, **2005,** *5*, 102-107.

39 Lee, J.N.; Park, C.; Whitesides, G.M. *Anal. Chem*. **2003,** *75*, 6544-6554.

40 Tsuda, T.; Sweedler, J. V.; Zare, R. N. *Anal.Chem.,* **1990,** *62,* 2149-2152.

41 Heiger, D. N.; Kaltenbach, P.; Sievert, H.-J. P. *Electrophoresis***, 1994**, *15*, 1234-1247.

42 Xue, Y.; Yeung, E. S. *Anal. Chem.*, **1994,** *66*, 3575-3580.

43 Bruin, G. J. M.; Stegeman, G.; Van Austen, A. C.; Xu, X.; Kraak, J. C.; Poppe, H. *J. Chromatogr.*, **1991,** *559*, 163-181.

44 Chervet, J. P.; Van Soest, R. E. J.; Ursem, M. *J. Chromatogr.*, **1991,** *543*, 439-449.

45 Mogensen, K. B.; Petersen, N. J.; Hu¨bner, J.; Kutter, J. P. *Electrophoresis*, **2001,** *22*, 3930-3938.

46 Petersen, N. J.; Mogensen, K. B.; Kutter, J. P. *Electrophoresis*, **2002,** *23*, 3528-3536.

47 Bean, S.R.; Lookhart, G.L**.,** *Cereal Chem.,* **2001,** *75*, 530-537.

48 Bean, S.R.; Lookhart, G.L**.,** *Electrophoresis*, **1998,** *19*, 3190-3198.

49 Lookhart, G.L.; Bean, S.R. *Cereal Chemistry* **1996,** *73*, 81-87**.**

50 Bean, S.R.; Lookhart, G.L. *Journal of Agricultural and Food Chemistry* **2000,** *48*, 344-353.

51 Bean, S.R.; Lookhart, G.L**.,** *Cereal Chem.,* **2001,** *75*, 530-537.

52 Bean, S.R.; Lookhart, G.L**.,** *Electrophoresis*, **1998,** *19*, 3190-3198.

53 Bean, S.R.; Lookhart, G.L**.,** *Cereal Chem.,* **2001,** *75*, 530-537.

54 Bean, S.R.; Lookhart, G.L**.,** *Electrophoresis*, **1998,** *19*, 3190-3198.

55 Lookhart, G.L.; Bean, S.R. *Cereal Chemistry* **1996,** *73*, 81-87**.**

56 Bean, S.R.; Lookhart, G.L. *Journal of Agricultural and Food Chemistry* **2000,** *48*, 344-353.

57 Sia, S.K.; Whitesides, G.M., *Electrophoresis,* **2003,** *24*, 3563-3576.

58 Moring, S.E.; Colburn, J.C.; Grossman, P.D.; Lauer, H.H. *LC-GC* **1990**, *8*, 34.

59 Tessmar JK, Gopferich AM. Customized PEG-derived copolymers for tissue-engineering applications. *Macromol Biosci.* **2007**, *7*, 23–39.

60 Towns J.K.; Regnier F.E. Capillary electrophoretic separations of proteins using nonionic surfactant coatings. *Anal Chem.* **1991,** *63*, 1126–1132.

61 Ullman, A. Formation and structure of self assembled monolayers. *Chem. Rev*. **1996,** *96*, 1533-1554.